Solvent-Induced Red-Shifts for the Proton Stretch Vibrational Frequency in a Hydrogen-Bonded Complex. I. A Valence Bond-Based Theoretical Approach.

ARTICLE *in* THE JOURNAL OF PHYSICAL CHEMISTRY B · MAY 2014

Impact Factor: 3.3 · DOI: 10.1021/jp501815j · Source: PubMed

4 AUTHORS, INCLUDING:

Philip Kiefer
University of Colorado Boulder
26 PUBLICATIONS **637** CITATIONS
SEE PROFILE

Ehud Pines
Ben-Gurion University of the Negev
83 PUBLICATIONS **2,683** CITATIONS
SEE PROFILE

James Hynes
University of Colorado Boulder
304 PUBLICATIONS **17,425** CITATIONS
SEE PROFILE

THE JOURNAL OF PHYSICAL CHEMISTRY B

Article

pubs.acs.org/JPCB

Solvent-Induced Red-Shifts for the Proton Stretch Vibrational Frequency in a Hydrogen-Bonded Complex. 1. A Valence Bond-Based Theoretical Approach

Philip M. Kiefer,*[,†] Ehud Pines,[‡] Dina Pines,[‡] and James T. Hynes*[,†,∥]

[†]Department of Chemistry and Biochemistry, University of Colorado, Boulder, Colorado 80309-0215, United States

[‡]Department of Chemistry, Ben-Gurion University of the Negev, P.O. Box 653, Be'er Sheva, 84105, Israel

[∥]Chemistry Department, École Normale Supérieure, UMR ENS-CNRS-UPMC 8640, 24 rue Lhomond, 75005 Paris, France

Supporting Information

ABSTRACT: A theory is presented for the proton stretch vibrational frequency ν_{AH} for hydrogen (H−) bonded complexes of the acid dissociation type, that is, AH···B ⇔ A^-···HB^+(but without complete proton transfer), in both polar and nonpolar solvents, with special attention given to the variation of ν_{AH} with the solvent's dielectric constant ε. The theory involves a valence bond (VB) model for the complex's electronic structure, quantization of the complex's proton and H-bond motions, and a solvent coordinate accounting for nonequilibrium solvation. A general prediction is that ν_{AH} decreases with increasing ε largely due to increased solvent stabilization of the ionic VB structure A^-···HB^+ relative to the neutral VB structure AH···B. Theoretical ν_{AH} versus $1/\varepsilon$ slope expressions are derived; these differ for polar and nonpolar solvents and allow analysis of the solvent dependence of ν_{AH}. The theory predicts that both polar and nonpolar slopes are determined by (i) a structure factor reflecting the complex's size/geometry, (ii) the complex's dipole moment in the ground vibrational state, and (iii) the dipole moment change in the transition, which especially reflects charge transfer and the solution phase proton potential shapes. The experimental proton frequency solvent dependence for several OH···O H-bonded complexes is successfully accounted for and analyzed with the theory.

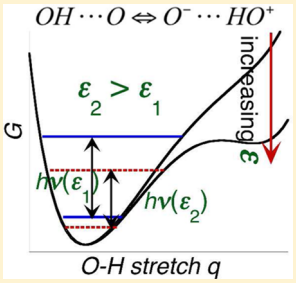

1. INTRODUCTION

Hydrogen (H−) bonding has long been of general interest; for example, in a reactivity context, it is of obvious importance for acid−base reactions in chemistry and biology,[1−9] with particular significance in proton transfer (PT) reactions[1−9] and biological catalysis.[9−11] An important characterization of H-bonds in solution involving a H-bond donor molecule AH has been via the proton vibrational AH stretch frequency ν_{AH},[1−8] in particular via the red-shift of ν_{AH} from its vacuum value. In this paper, we construct a theory for this red-shift and apply it to recent vibrational spectroscopic experimental results for H-bonded complexes in solution.

In a molecular perspective, this vibrational red-shift is related to the H-bond formation enthalpy (H-bond strength) of the H-bond formed with a solvent molecule S, for example, AH···S.[1−8] This specific interaction is one component of the semiempirical Kamlet−Taft analyses,[12−16] which have frequently been used to decompose different effects for H-bonds, including specific and general solvent polarity effects. Unfortunately, such analyses have had only limited success in the proton vibrational problem.[12−16] A conceptually different and theoretical approach foregoes any inclusion of specific molecular interactions and focuses on the solute, here AH, immersed in a solvent described as an equilibrium dielectric continuum; that is, the H-bond acceptor molecule is not treated microscopically. Most theories[17−19] in this vein derive from the original work of Kirkwood[17] and predict a red-shift on the basis of the proportional relationship between a molecular dipole moment, μ, inside an Onsager spherical cavity,[20,21] and the solvent's equilibrium dielectric reaction field. This approach describes the vibrational red-shift in terms of a function of the solvent's static dielectric constant, ε, and correctly predicts the overall feature that the frequency increasingly red-shifts with an increase in solvent polarity.[1−8,18,19,22−25]

Buckingham[22] and Pullin[23−25] expanded on the Kirkwood approach in several important ways. First, the vibrational coordinate dependence of the dipole moment μ in the solute−solvent interaction was taken into account (similar solvation effects on the potential have been incorporated with quantum chemistry methods[26−29]). Next, some, but not all, aspects of the equilibrium assumption for the solvent's nuclear polarization were removed. Further, the solute vacuum potential anharmonicity was treated via perturbation theory, either quantum[22] or classical;[23,24] such an approximation, while reasonable for many vibrations, can be questioned for very anharmonic proton coordinate vibrations. Finally, the Buckingham−Pullin approach has been combined with the van der Zwan−Hynes[30] time-dependent solvation dynamics description to include

Special Issue: James L. Skinner Festschrift

Received: February 20, 2014
Revised: May 1, 2014
Published: May 7, 2014

aspects of nonequilibrium solvation for the solvent nuclear polarization. This approach, which was first applied to vibrations by Lian and co-workers[31], has been employed by Batista, Nibbering, and co-workers to compare OH red-shifts in the ground and electronic states of photoacids in solution.[32,33]

In the above, we have mentioned a few of the limitations of prior approaches to the vibrational red-shift for H-bonded complexes in solution, and others will be discussed near the end of this paper. Here, we stress that the theory, which we develop within, has a number of features that contrast with the various approaches mentioned above. Some, though not all, aspects of the theory have been used in previous PT work.[34−40]

(1) The theory focuses from the beginning on the proton frequency (e.g., ν_{AH}) in *intact* H-bonded complexes, that is, both the H-bond donor (AH) and acceptor base (B) molecules are treated molecularly, within the complex, itself immersed in a solvent. This captures the very important, indeed dominant, effect of the interaction between the H-bond molecular pair. (Pullin[23] has already indicated the inappropriate character of application of Kirkwood-type theories to solutes with strong specific interactions with the solvent.) Our focus is on H-bonded complexes of interest of the acid dissociation type but without complete PT.

(2) It also emphasizes the charge transfer contribution to the H-bond interaction within the complex[1−8,38,41−46] via a 2-state valence bond (VB) model involving the VB structures

$$AH\cdots B \leftrightarrow A^{-}\cdots HB^{+} \quad (1)$$

A large change in dipole moment between these neutral and ionic structures promotes a measurable change in the proton potential with changing solvent. The VB description also proves to be important in relating the red-shift to acidity (and related charge transfer) issues, such as the difference of proton affinities of the base B and the conjugate base A^- of the acid AH. This VB model has previously been shown useful in describing solvent polarity effects for H-bond structures and PT reactions,[40] as well as frequency shifts of gas phase H-bonded complexes.[38]

(3) In the theory, both the proton and H-bond nuclear coordinate motions, which are very strongly coupled,[1−8] are quantized. This is an especially important aspect for the calculation of ν_{AH} for vibration in the very anharmonic proton potential, and it avoids frequency assessment by the curvature at the bottom of a potential or free energy well. The inclusion of the strongly coupled H-bond vibration allows the H-bond length change that accompanies a change in H-bond strength with a change in solvation, with important consequences for the red-shift.

(4) A nonequilibrium dielectric continuum description for the surrounding solvent is employed. While the solvent's electronic polarization (associated with the optical ε_∞ dielectric constant) is assumed to always be in equilibrium with the rapid proton motion and during the vibrational transition, the solvent's nuclear (mainly orientational) polarization is out of equilibrium both with that proton motion and during that Franck−Condon transition; this is associated with the difference between ε_∞ and the static dielectric constant ε. In this connection, nonpolar and polar solvents will be shown to have different red-shift behavior. The theory requires some limited explicit electronic structure calculations for the H-bonded complexes in a model nonpolar solvent for its implementation for both nonpolar and polar solvents.

(5) With the above ingredients, the theory is couched in terms of the nonequilibrium free energy, G, for the combined H-bonded complex and the surrounding solvent. G depends on the proton and H-bond coordinates of the complex and the nonequilibrium solvent orientational polarization, which is characterized by a solvent coordinate, s. Time scale arguments for the various coordinates and the Franck−Condon principle for the vibrational transition permit the calculation of the vibrational frequency ν_{AH} from the appropriate proton potential.

This theory is applied here to recent experiments that isolate the solvent's influence on ν_{AH} from the influence of the specific interaction within the H-bonded complex.[18] In these experiments, this is accomplished by keeping the acid−base H-bond pair the same while the solvent is varied, so that the specific H-bond interactions' contribution is practically constant. Using the base dimethyl sulfoxide (DMSO) ensures that the only H-bond present in solution is an acid-complexing base 1:1 complex not containing a solvent molecule. A key point here is that these constraints allow a ν_{AH} interpretation in terms of a single, albeit averaged, H-bond structure,[47] removing possible non-Condon effects arising from multiple equilibrium H-bond configurations.[49,50]

Figure 1 displays the measured proton stretch frequency ν_{OH} versus the inverse solvent static dielectric constant $1/\varepsilon$ for

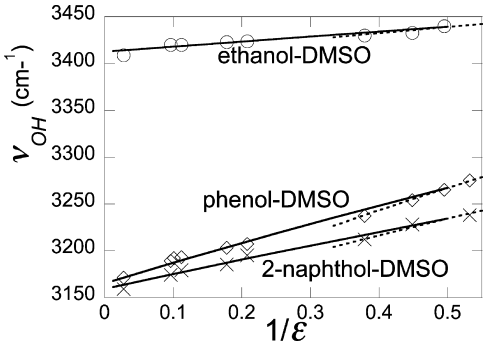

Figure 1. OH vibrational stretch frequency $\nu_{AH} = \nu_{OH}$ versus the inverse of the static dielectric constant $1/\varepsilon$ for ethanol−DMSO (○), phenol−DMSO (×), and 2-naphthol−DMSO (◇) complexes. Lines indicate the polar (solid line) and nonpolar (dotted line) solvent theoretical formalism described in section 5.1; the high frequency dielectric constant is taken to be equal to 2 for the polar solvent curve. Experimental data are taken from ref 18. Solvents from lowest ε to highest ε are hexane, cyclohexane, CCl_4, CS_2, chloroform, chlorobenzene, dichloromethane, 1,2-dichlorobenzene, 1,2-dichloroethane, and acetonitrile. The first four solvents are nonpolar solvents with $\varepsilon = \varepsilon_\infty$ and $1/\varepsilon > 0.3$, and the remainder are polar solvents.[51,52] Ethanol−DMSO data are absent for hexane and 1,2-dichlorobenzene, while 2-naphthol−DMSO data are absent for cyclohexane and 1,2-dichlorobenzene. Table 1 lists the static ε and optical dielectric ε_∞ constants for the solvents.[51,52]

ethanol (C_2H_5OH), phenol (C_6H_5OH), and 2-naphthol ($C_{10}H_7OH$) complexed with the base DMSO.[18] The two lines for each complex distinguish the predicted theoretical trends for nonpolar and polar solvents, for which static and high frequency dielectric constants are listed in Table 1. Nonpolar solvents (those in Figure 1 with $1/\varepsilon > 0.3$) are defined as having no net molecular permanent dipole moment, such that ε is essentially identical to the high frequency dielectric constant ε_∞, that is, $\varepsilon \approx \varepsilon_\infty$, arising from the electronic polarization, which itself is very close to the square of

dx.doi.org/10.1021/jp501815j | J. Phys. Chem. B 2014, 118, 8330−8351

Table 1. Polar and Nonpolar Solvents ε and Their Static and Optical ε_∞ Dielectric Constants[a]

solvent	ε[b]	$\varepsilon_\infty = n^2$[c]
hexane	1.88	1.89
cyclohexane	2.02	2.02
CCl_4	2.23	2.13
CS_2	2.64	2.65
chloroform	4.81	2.09
chlorobenzene	5.62	2.32
dichloromethane	8.93	2.03
1,2-dichlorobenzene	9.90	2.41
1,2-dichloroethane	10.37	2.09
acetonitrile	35.94	1.81

[a]The first four entries are considered nonpolar solvents with $\varepsilon \sim \varepsilon_\infty$, while the remainder are polar solvents. [b]Taken from refs 51 and 52. [c]The optical dielectric constant ε_∞ is equivalent to the square of the refractive index n.[51,52]

the index of refraction (cf. Table 1). Polar solvents have a nonzero net permanent dipole moment and a static dielectric constant $\varepsilon > \varepsilon_\infty$, due to both orientational and electronic polarization.

In this work, we will develop and apply the theory of which results are illustrated in Figure 1 with a special focus on the influence of the solvent, proton potential anharmonicity, the H-bonded complex geometry and charge distribution, and charge transfer.

The outline of the remainder of this paper is as follows. Section 2 presents the 2 VB state nonequilibrium solvation formalism for an H-bonded complex solute embedded in a dielectric continuum, including a description of the solvent's two types of electrical polarization and the free energy surface, G, dependent on both solute nuclear coordinates and a solvent coordinate. Section 3 is devoted to deriving the theoretical expressions for the proton frequency, ν_{AH}, and its variation with the inverse of the solvent dielectric constant $1/\varepsilon$. We focus first on the theory development for the polar solvent case because it is considerably more general and of most practical interest. With that accomplished, the nonpolar solvent case theory formulation for ν_{AH} and its variation with $1/\varepsilon$ is addressed. Section 4 deals with the evaluation of properties of the H-bonded complexes needed to evaluate the theoretical model, including their structure and geometries, VB state potentials, and dipole moments. Some limited electronic structure calculations are involved here for the complexes immersed in a reference nonpolar solvent. An important point here is that model parametrizations derived for the nonpolar solvent case are also used for the polar solvent situation. Section 5 is devoted to the theoretical evaluation, analysis, and interpretation of the curves displayed in Figure 1 in comparison with the experimental results, including a numerical validation of the ν_{AH} versus $1/\varepsilon$ slope expressions derived in section 3. Concluding remarks are offered in section 6. Several aspects of the potentials and the free energies are given in Appendix A, Appendix B, and Supporting Information.

2. THEORETICAL FORMALISM: HAMILTONIAN AND FREE ENERGY

We begin with the H-bonded complex in a polar solvent case, and later specialize when necessary to the more simple nonpolar solvent situation. In our treatment of the vibrational problem, the system's quantum Hamiltonian is given by the sum of the nuclear kinetic energy operator $\hat{K}_{q,Q}$, the classical solvent kinetic energy K_s, and a free energy $G(q,Q,s)$[34−37]

$$\hat{H} = \hat{K}_{q,Q} + K_s + G(q, Q, s) \tag{2}$$

involving the two nuclear coordinates of the H-bonded complex, the A−H separation q and the A−B separation Q, both treated quantum mechanically, and finally a classical solvent coordinate s. This last coordinate can be thought of as gauging the solvent's electrical orientational polarization state. The free energy surface $G(q,Q,s)$ acts, as in other problems,[53−60] as an effective system potential energy. In this section, we present the ingredients necessary for obtaining the appropriate free energy surface for the vibrational problem, to then be used with eq 2 in section 3 to obtain the proton stretch vibrational frequency and its solvent dependence.

2.1. Electronic Structure Description. We first need to consider the electronic structure of the H-bonded complex. This is described by a wave function Ψ

$$\Psi(q, Q, s) = c_N(q, Q, s)\psi_N(q, Q) + c_I(q, Q, s)\psi_I(q, Q) \tag{3}$$

which is a superposition of two charge-localized VB wave functions corresponding to the neutral (N) and ionic (I) pair states in eq 1. The expansion coefficients depend on the complex's two nuclear coordinates, the A−H separation, q, and the A−B separation, Q, as well as on the solvent coordinate, s, to be defined later. The latter's presence reflects the important feature that the solvent electrical polarization can polarize the solute's electronic structure over these VB states. Associated with each VB state is a vacuum potential energy, V_N and V_I, respectively, to be defined later. The two VB states are strongly coupled by a large electronic coupling β (∼1 eV[35−37,61]), such that the system is completely electronically adiabatic. As will be seen in section 2.2, this mixing of diabatic states must be performed in the presence of the solvent, which leads to the electronically adiabatic free energy surface $G(q,Q,s)$.

The H-bonded complex in a solvent will be electrostatically described by a finite dipole $\boldsymbol{\mu}(q,Q)$ within a cavity immersed in a dielectric continuum;[34−37,39,62] this dipole moment, which depends on the complex's nuclear coordinates, will be more fully characterized immediately below and in section 4.2. The bare electric field produced by the solute and experienced by the solvent at the vector point r is given by the dipolar field

$$\mathbf{E}_{\boldsymbol{\mu}}(q, Q, s, \mathbf{r}) = \langle\Psi| - \nabla\boldsymbol{\mu}(q, Q)\cdot\mathbf{r}/r^3|\Psi\rangle = \langle\Psi|\boldsymbol{\mu}(q, Q)|\Psi\rangle\cdot\overline{\overline{\mathbf{T}}}(\mathbf{r}) = \boldsymbol{\mu}(q, Q, s)\cdot\overline{\overline{\mathbf{T}}}(\mathbf{r}) \tag{4}$$

where $\overline{\overline{\mathbf{T}}}$ is the dipole tensor. The solvent coordinate dependence of the bare fields arises from the s-dependence of the electronic wave function (eq 3) in the quantum electronic structure-averaged dipole moment $\boldsymbol{\mu}(q,Q,s)$; the bare fields are thus vacuum fields but with the complex's charges influenced by polarization state of the solvent. Hereafter, we will assume that the dipole moments $\boldsymbol{\mu}(q,Q)$ and its diabatic components lie along a single axis in the complex; with the solvent coordinate dependence arising from that of the VB state coefficients, the magnitude $\mu(q,Q,s)$ of the averaged dipole moment is defined in terms of the diabatic dipole moments $\mu_N(q,Q)$ and $\mu_I(q,Q)$[63] as

$$\mu(q, Q, s) \equiv \langle\Psi|\mu|\Psi\rangle = c_N^2(q, Q, s)\mu_N(q, Q) + c_I^2(q, Q, s)\mu_I(q, Q) \quad (5)$$

where we have neglected a small transition dipole moment contribution.[64] The bare electric field $\boldsymbol{E}_\mu$ can be similarly written in terms of the s-independent diabatic VB state fields $\boldsymbol{E}_N(q,Q;r)$ and $\boldsymbol{E}_I(q,Q;r)$[34]

$$\boldsymbol{E}_{\boldsymbol{\mu}}(q, Q, s; \mathbf{r}) = c_N^2(q, Q, s)\boldsymbol{E}_{\mathbf{N}}(q, Q; \mathbf{r}) + c_I^2(q, Q, s)\boldsymbol{E}_{\mathbf{I}}(q, Q; \mathbf{r}) \quad (6)$$

The VB electric fields are bare and vacuum fields at the same time because the VB state charge distributions themselves are independent of the solvent's polarization state.

As will be seen below, associated with each VB state field interaction is the scalar structure factor, M_S, defined by the integral over the solvent outside the solute cavity[34]

$$M_S = \frac{1}{8\pi}\int d^3r\hat{\boldsymbol{e}}\cdot\overline{\overline{\mathbf{T}}}(\mathbf{r})\cdot\overline{\overline{\mathbf{T}}}(\mathbf{r})\cdot\hat{\boldsymbol{e}} \quad (7)$$

where $\hat{\boldsymbol{e}}$ is a unit vector along the H-bonded complex axis.

2.2. Solvent Polarization and the Solvent Coordinate.

The H-bonded complex−solvent interaction depends on the electric fields defined above and the solvent electrical polarization. In a broad view, the solvent polarity characterized by the static dielectric constant ε will affect the neutral and ionic composition of the complex's electronic structure (via the coefficients in eq 3, e.g., increasing the weight of the ionic state with increasing ε); this will distort (soften) the potential energy curve for the H vibration, thereby influencing (red-shifting) the vibrational frequency.

A detailed examination of the solvent polarity effect must start at a more fundamental level and pay attention to several time scale issues. The first is that the solvent electrons are fast compared to the q and Q nuclear motion in the complex. The second is that, in the vibrational transition, the solvent electrons will "instantly" adjust, but according to the Franck−Condon Principle, the solvent nuclei will not. The third is that the coupled nuclear degrees of freedom of the solvent are slow compared to the high frequency q proton motion and often slow compared to the H-bond coordinate Q motion;[65] this situation is in complete contrast to any treatment that assumes the solvent is equilibrated, for example, to proton motion at any given q value, an assumption of some alternate approaches.[66−69]

Within the dielectric continuum solvent framework which we employ, these considerations require the use of a nonequilibrium description for the surrounding solvent, where the solvent molecules and their electron distributions are characterized by two solvent vector fields: the electronic $\boldsymbol{P}_e(\boldsymbol{r})$ and rotational or orientational $\boldsymbol{P}_{or}(\boldsymbol{r})$ polarizations, respectively.[34,53−55] There is equilibrium for the first type of solvent polarization. The rapidity of the solvent electrons, which can follow and equilibrate to the proton coordinate (and a fortiori the H-bond coordinate), results in the vacuum potentials V_N and V_I for the VB states being altered by the equilibrium solvation associated with $\boldsymbol{P}_e(\boldsymbol{r})$ to the free energies

$$G_{N,I}^{\infty}(q, Q) = V_{N,I}(q, Q) - \frac{1}{2}K_\infty\mu_{N,I}^2(q, Q) \quad (8)$$

where the "force constant" for the electronic polarization is

$$K_\infty = 2M_S\left(1 - \frac{1}{\varepsilon_\infty}\right) \quad (9)$$

with the factor $(1 - 1/\varepsilon_\infty)$ reflecting the equilibrium condition for that polarization. Here, ε_∞ is the high frequency solvent dielectric constant, and M_S is the structure factor eq 7. In fact, the equilibrium electronic polarization solvation in eq 8 will distort the vacuum vibrational potentials, for example, the neutral state dipole $\mu_N(q,Q)$ will increase with greater proton extension, increasing the proton potential's anharmonicity. For continuum nonpolar solvents, where $\varepsilon = \varepsilon_\infty = 2$,[51,52] electrostatic solvation is exclusively due to solvent electronic polarization.

On the other hand, the solvent orientational polarization ($\boldsymbol{P}_{or}$) field is not so equilibrated to the faster solute degrees of freedom q and Q.[65] Thus, we require a free energy expression for a given, generally *nonequilibrium* $\boldsymbol{P}_{or}$. The discussion of this will proceed most easily by considering the contribution to the total free energy dependent on this polarization, that is, the free energy of interaction and self-free energy of the solvent $\boldsymbol{P}_{or}$ in the presence of a VB state vacuum electric field $\boldsymbol{E}_N$ or $\boldsymbol{E}_I$:[34,53−57]

$$G_{int,N,I} + G_{self} = -\frac{1}{\varepsilon_\infty}\int d^3r\boldsymbol{E}_{N,I}(\boldsymbol{r})\cdot\boldsymbol{P}_{or}(\boldsymbol{r}) + \frac{1}{2}\frac{4\pi\varepsilon_o}{\varepsilon_\infty(\varepsilon - \varepsilon_\infty)}\int d^3r\boldsymbol{P}_{or}(\boldsymbol{r})\cdot\boldsymbol{P}_{or}(\boldsymbol{r}) \quad (10)$$

In this formulation, the integrals are over the surrounding solvent outside of the cavity and boundary conditions are ignored[34,36,37,53−57,70,71] (as they also are in M_S, eq 7). We return to this point after eq 14 below.

As in other problems,[34,53−60] we will replace the characterization of the full $\boldsymbol{P}_{or}$ field by a single scalar solvent coordinate s. In view of the time scale considerations set forth at the beginning of this subsection, this requires a certain care for the H-bonded complex vibrational problem. We seek a nonequilibrium solvent coordinate, s, which in effect interpolates between the solvent being in (appropriate) equilibrium with the fields of the two VB states. A key point here is that those fields depend on the solute coordinates q and Q, which are fast compared to the solvent orientational polarization and whose motion is quantized. The appropriate equilibrium limits then should involve equilibration to *quantized* fields, and the quantization should be done in the complex's ground vibrational state, from which the proton stretch vibrational transition occurs. Accordingly we write

$$\begin{aligned}\boldsymbol{P}_{or}(\boldsymbol{r}) &= \frac{\varepsilon_\infty}{4\pi}\left(\frac{1}{\varepsilon_\infty} - \frac{1}{\varepsilon_o}\right)[(1 - s)\langle\phi_{0,Neq}(q, Q)|\boldsymbol{E}_{\mathbf{N}}(q, Q; \mathbf{r})|\phi_{0,Neq}(q, Q)\rangle + s\langle\phi_{0,Ieq}(q, Q)|\boldsymbol{E}_{\mathbf{I}}(q, Q; \mathbf{r})|\phi_{0,Ieq}(q, Q)\rangle] \\ &\equiv \frac{\varepsilon_\infty}{4\pi}\left(\frac{1}{\varepsilon_\infty} - \frac{1}{\varepsilon}\right)[(1 - s)\langle\boldsymbol{E}_{\mathbf{N}}(q, Q; \mathbf{r})\rangle_{0,Neq} + s\langle\boldsymbol{E}_{\mathbf{I}}(q, Q; \mathbf{r})\rangle_{0,Ieq}]\end{aligned} \quad (11)$$

in which the prefactor involving the difference of inverse dielectric constants reflects the equilibrium orientational polarization structure, with the solvent coordinate s reflecting the polarization's nonequilibrium character. Here, the brackets in the first line indicate quantum nuclear averages, over a vibrational wave function, in the ground vibrational state with

dx.doi.org/10.1021/jp501815j | J. Phys. Chem. B 2014, 118, 8330−8351

the solvent orientational polarization $\boldsymbol{P}_{or}$ equilibrated to the relevant quantized VB state electric field. (The actual procedure to characterize such equilibrium conditions will be described in section 3.1.) It is seen that $s = 0$ corresponds to the orientational polarization being equilibrated to the neutral VB state, while $s = 1$ corresponds to it being equilibrated to the ionic VB state, with the complex's nuclear coordinates quantized in each of those states. In addition, s is independent of the solute coordinates, an important aspect that allows us to treat it as an independent variable.

With the relations

$$\langle \mathbf{E}_{N,I} \rangle_{0,Neq,Ieq} = \overline{\overline{\mathbf{T}}} \cdot \langle \boldsymbol{\mu}_{N,I} \rangle_{0,Neq,Ieq} \tag{12}$$

connecting the nuclear averages of the VB state electric fields and the VB state dipole moments, the combination of eqs 10 and 11, and the structure factor definition eq 7, the sum of the interaction and self-free energies for each of the VB states is now expressed as

$$\begin{aligned} &G_{int,N,I}(q, Q, s) + G_{self}(s) \\ &\quad = -K\mu_{N,I}(q, Q)[(1 - s)\tilde{\mu}_N + s\tilde{\mu}_I] \\ &\qquad + \frac{K}{2}[(1 - s)\tilde{\mu}_N + s\tilde{\mu}_I]^2 \end{aligned} \tag{13}$$

in which K is the force constant for solvent orientational polarization

$$K = 2M_S\left(\frac{1}{\varepsilon_\infty} - \frac{1}{\varepsilon}\right) \tag{14}$$

whose dependence on the inverse dielectric constant difference reflects the same factor in the orientational polarization eq 11. In eq 13, $\tilde{\mu}_N$ and $\tilde{\mu}_I$ are the quantum-averaged ground vibrational state VB dipole moment magnitudes

$$\tilde{\mu}_{N,I} \equiv \langle \mu_{N,I} \rangle_{0,Neq,Ieq} \tag{15}$$

which are obviously independent of q and Q.

We noted below eq 10 that the free energy formulation we use[34,36,37,53−57] and the structure factor M_S (eq 7) involve integrals in which boundary conditions are ignored. The only relevant consequences for the theoretical description under construction are two. The first is the appearance of inverse dielectric constant difference factors in the force constants eqs 9 and 14. These factors are familiar, for example, from the Marcus formulation for the activation free energy for electron transfer reactions[70−72] and there reflects an approximate description of separate charges; in the present case, it reflects the related approximate description of a finite dipole moment, dependent on the H-bonded complex's nuclear coordinates.[73] The second is that we will need to evaluate the structure factor M_S not from eq 7 but from a reference accurate free energy; this is discussed in section 4.4.

In closing this subsection, we point out that there is an instructive way to rewrite eq 13, which recognizes that

$$\mathcal{R}(s) = K[(1 - s)\tilde{\mu}_N + s\tilde{\mu}_I] = K[\tilde{\mu}_N + s(\tilde{\mu}_I - \tilde{\mu}_N)] \tag{16}$$

is the equilibrium (orientational) *reaction field*[34,53−55] for the s-dependent dipole moment

$$\tilde{\mu}(s) = \tilde{\mu}_N + s(\tilde{\mu}_I - \tilde{\mu}_N) \tag{17}$$

In general, $\mathcal{R}$ is a *nonequilibrium* quantity because the actual H-bonded complex's dipole moment is generally *not* $\tilde{\mu}(s)$.[30] Instead, it is the quantum ground state vibrational average of $\mu = c_N^2\mu_N + c_I^2\mu_I$; see eq 5 and the discussion below it. When the reaction field is that appropriate to (i.e., equilibrated to) the complex's actual quantum-averaged dipole moment, we label it $\mathcal{R}_{eq}$. In terms of this nonequilibrium reaction field, eq 13 takes the form we will now employ

$$G_{int,N,I}(q, Q, s) + G_{self}(s) = -\mu_{N,I}(q, Q)\mathcal{R}(s) + \frac{K}{2}\mathcal{R}(s)^2 \tag{18}$$

2.3. Free Energy Surface $G(q,Q,s)$. We now turn to the expression for the full free energy surface $G(q,Q,s)$. Its derivation is essentially identical to that presented elsewhere,[34,36,37,39] and not repeated here. $G(q,Q,s)$ has the structure of the individual VB state free energy surfaces $G_N(q,Q,s)$ and $G_I(q,Q,s)$ coupled by the electronic resonance coupling $\beta(Q)$ introduced near the beginning of section 2.1,

$$\begin{aligned} G(q, Q, s) = {} & [G_N(q, Q, s) + G_I(q, Q, s)]/2 \\ & - \frac{1}{2}\sqrt{(G_I(q, Q, s) - G_N(q, Q, s))^2 + 4\beta(Q)^2} \end{aligned} \tag{19}$$

where we have anticipated that the resonance coupling is predominantly a function of the H-bond coordinate Q.[36,37,39,74,75] This equation has the same basic structure as the lower electronically adiabatic energy level for two coupled diabatic levels. The VB state free energies $G_{N,I}$ are the appropriate sums of the vacuum potentials modified by equilibrium solvation by the electronic polarization[34,53−55,65] eq 8, and by the interaction and self-free energies eq 18:

$$\begin{aligned} G_{N,I}(q, Q, s) &= G^{\infty}_{N,I}(q, Q) + G_{int,N,I}(q, Q, s) + G_{self}(s) \\ &= V_{N,I}(q, Q) - \frac{1}{2}K_\infty\mu^2_{N,I}(q, Q) - \mu_{N,I}(q, Q)\mathcal{R}(s) \\ &\quad + \frac{1}{2K}\mathcal{R}(s)^2 \end{aligned} \tag{20}$$

The VB state coefficients in the H-Bonded complex's electronic wave function eq 3 for the ground electronic state are given in terms of the VB free energies $G_{N,I}(q,Q,s)$ by[34,36,37,53−55]

$$c^2_{N,I}(q, Q, s) = \frac{1}{2} \pm \frac{1}{2}\frac{(G_I(q, Q, s) - G_N(q, Q, s))}{\sqrt{(G_I(q, Q, s) - G_N(q, Q, s))^2 + 4\beta^2(Q)}} \tag{21}$$

showing that the complex's electronic structure depends on the solvent coordinate via the VB state free energy difference. These coefficients are important for the vibrational problem: they explicitly carry the H-bonded complex's electronic structure information.

3. THEORETICAL FORMULATION: PROTON VIBRATIONAL FREQUENCY AND ITS DEPENDENCE ON SOLVENT DIELECTRIC PROPERTIES

3.1. Proton Vibrational Frequency. We can now obtain the desired proton vibrational frequency (recall that we are still dealing with the H-bonded complex in the polar solvent situation). We have already constructed the free energy surface $G(q,Q,s)$, eqs 19 and 20, which serves as the effective potential energy surface for the quantum Hamiltonian eq 2, which we rewrite here for convenience:

dx.doi.org/10.1021/jp501815j | J. Phys. Chem. B 2014, 118, 8330−8351

$$\hat{H} = \hat{K}_{q,Q} + K_s + G(q, Q, s) \tag{22}$$

Recall from section 2.2 that the H-bonded complex coordinates q and Q are taken to be fast compared to the solvent orientational polarization, here parametrized via the solvent coordinate s via eq 11. Accordingly, the quantization of the q and Q motion must be effected at a fixed s value with the effective potential energy surface for this quantization taken as $G(q,Q,s)$

$$(\hat{K}_{q,Q} + G(q, Q, s))|\phi_n(q, Q, s)\rangle = G_n(s)|\phi_n(q, Q, s)\rangle \tag{23}$$

where ϕ_n is the vibrational eigenfunction of the Hamiltonian operator $\hat{H}$ (without K_s) with free energy eigenvalue $G_n(s)$.

The quantized energy levels $\mathcal{E}_n(s)$ of the nuclear vibrational motion are obtained by subtracting the free energy minimum $G_{min}(q_{min},Q_{min},s)$, which provides a common zero of energy for each vibrational state, from the free energy eigenvalues $G_n(s)$ for a given s[76]

$$\mathcal{E}_n(s) = G_n(s) - G_{min}(q_{min}, Q_{min}, s) \tag{24}$$

where the minimum values $q_{min}(s)$ and $Q_{min}(s)$ characterizing the minimum G value at a given s are determined from the conditions[34,53−55]

$$\frac{\partial G(q, Q, s)}{\partial q} = 0; \quad \frac{\partial G(q, Q, s)}{\partial Q} = 0 \tag{25}$$

Our major goal for the proton vibrational problem is of course the absorption frequency ν_{AH}, determined by the energy gap $h\nu_{AH}$ between the first and excited vibrational state for a given s

$$h\nu_{AH}(s) = \mathcal{E}_1(s) - \mathcal{E}_0(s) \tag{26}$$

But because $G_{min}(q_{min},Q_{min},s)$ in eq 24 is the same for every vibrational state and $h\nu_{AH}$ is a difference of energy levels, G_{min} will cancel out, and we can ignore it in the following development. The absorption frequency at a given s can thus be generalized as a difference in expectation values (first excited minus ground) of the Hamiltonian in eq 22

$$\begin{aligned} h\nu_{AH}(s) &= \langle\phi_1(q, Q, s)|\hat{H}|\phi_1(q, Q, s)\rangle - \langle\phi_0(q, Q, s)|\hat{H}|\phi_0(q, Q, s)\rangle \\ &\equiv \langle\hat{K}_{q,Q} + G(q, Q, s)\rangle_1 - \langle\hat{K}_{q,Q} + G(q, Q, s)\rangle_0 \\ &= G_1(s) - G_0(s) \end{aligned} \tag{27}$$

where the classical solvent kinetic energy K_s has also canceled out.

The last consideration needed before writing our desired final equation for $h\nu_{AH}$ is that the IR absorption occurs from an initial equilibrium ground vibrational state. As emphasized in section 2, this equilibrium does *not* involve equilibration of the solvent orientational polarization with the H-bonded complex's q and Q coordinates. Instead, the quantization must be effected at fixed solvent coordinate s values, as in our development so far. The appropriate ground state equilibrium condition is that of the minimum of the ground vibrational free energy curve $G_0(s)$

$$\frac{dG_0(s)}{ds} = 0; \quad s = s_{eq0} \tag{28}$$

which defines the ground vibrational state equilibrium solvent coordinate s_{eq0}. Figure 2a illustrates $h\nu_{AH}$ for two different s_{eq0} values, while Figure 2b illustrates the variation of s_{eq0} locations with varying solvent dielectric constant. (The H-bond separation Q in Figure 2a is kept fixed only for simplicity.)[80]

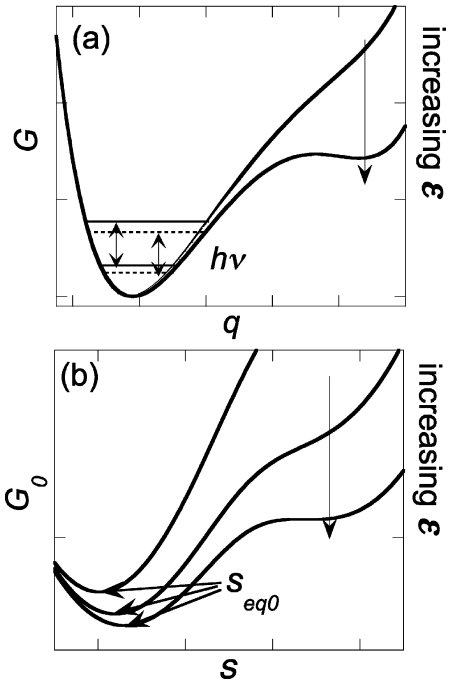

Figure 2. (a) Free energy proton potentials versus the proton position q for two ε values for a fixed H-bond separation Q. The ground and excited A−H stretch states are indicated as solid lines for the smaller ε and dashed lines for the higher ε. (b) Depiction of the vibrational ground state free energy G_0 versus the solvent coordinate s for three solvent dielectric constant ε values, with the equilibrium solvent coordinate s_{eq0} indicated.

We now find s_{eq0}. Differentiation of eq 23, using the Hellman−Feynman theorem[83] (the ground vibrational state wave function $\phi_0(q,Q,s)$ is normalized to unity in the q and Q coordinates) gives

$$\frac{dG_0(s)}{ds} = \langle\phi_0(q, Q, s)\left|\frac{dG(q, Q, s)}{ds}\right|\phi_0(q, Q, s)\rangle = 0 \tag{29}$$

which yields, after some manipulation (see Appendix A), the equilibrium solvent position

$$s_{eq0} = \frac{\langle\mu\rangle_{eq0} - \tilde{\mu}_N}{\tilde{\mu}_I - \tilde{\mu}_N} \tag{30}$$

(One can check, using eq 15 for $\tilde{\mu}_N$ and $\tilde{\mu}_I$, that eq 30 properly reduces to 0 and 1, respectively, for a purely neutral or ionic VB state.) Because the solvent coordinate for the excited vibrational state must remain the same as in the ground state by the Franck−Condon principle, our final general equation of the absorption frequency is then simply eq 27 evaluated at $s = s_{eq0}$:

$$h\nu_{AH}(s_{eq0}) = \mathcal{E}_1(s_{eq0}) - \mathcal{E}_0(s_{eq0}) = G_1(s_{eq0}) - G_0(s_{eq0}) \tag{31}$$

Figure 2b depicts three $G_0(s)$ curves with differing static dielectric constant ε. An important feature there is that s_{eq0} increases as ε increases. The ionic character of the complex increases, via eq 30: as ε increases, the ionic VB state is stabilized more relative to the neutral state due to the increased solvation free energy of the ionic complex. The consequences

dx.doi.org/10.1021/jp501815j | J. Phys. Chem. B 2014, 118, 8330−8351

of the ionic state's relative stabilization for the H-bond potential, from which ν_{AH} is derived, is semiquantitatively depicted in Figure 2a. There, it is seen that an increased ionic contribution to the proton potential for larger q with increasing ε increases the anharmonicity of the potential. The result is a decrease in ν_{AH} as $1/\varepsilon$ decreases (Figure 1).

The characterization of the proton stretch is in fact a two-dimensional Q and q vibrational problem. As is well-known,[1−8] a significant coupling exists between q and the H-bond length Q, necessitating the quantization of a two-dimensional vibration. For our calculations, this two-coordinate quantization is carried out simultaneously,[35−38] but a simpler discussion will help in comprehending the q−Q coupling effects we will encounter in our subsequent discussion. The q variation of the effective potential and associated vibrational levels are easily visualized for a given H-bond length Q_{eq0}, as depicted in Figure 2a. The influence of the H-bond coordinate Q is indicated in Figure 3, which depicts the nuclear free energy potential G

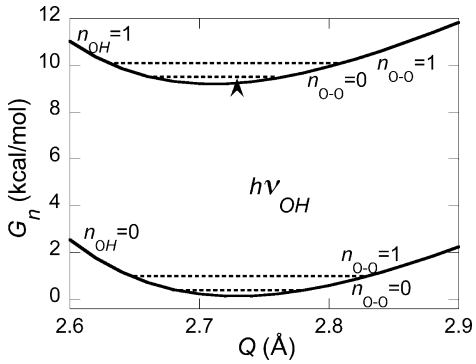

Figure 3. Free energy $G(q,Q,s)$ for a given s versus the H-bond length Q with the proton stretch quantized in its ground $n_{OH} = 0$ and excited $n_{OH} = 1$ states (solid lines) for the phenol−DMSO complex. Dashed lines indicate ground and excited H-bond vibrational states from subsequent quantization of the H-bond mode. The arrow indicates the dominant transition in the OH vibrational spectrum from $n_{OH} = 0$ to $n_{OH} = 1$, with the H-bond mode quantized in its ground vibrational state $n_{O-O} = 0$. The simplified quantization method for this figure (described in the text) differs from the simultaneous quantization of q and Q employed for the frequency calculations herein.

versus Q for an equilibrium solvent position s_{eq0} for the phenol−DMSO complex. The proton stretch coordinate q here has been quantized for each H-bond separation for simplicity and ease of visualization. The two Q displayed potentials correspond to q quantized in the ground ($n_{OH} = 0$) and excited ($n_{OH} = 1$) OH stretch vibrational states. As expected, the latter's equilibrium O−O separation is noticeably shorter than that of the former's.[84,85] Figure 3 also displays the ground and first excited Q vibrational states ($n_{OO} = 0$ and 1), with $h\nu_{OH}$ depicted for the $n_{OH} = 0$ to $n_{OH} = 1$ transition with $n_{OO} = 0$. Obviously, transitions between other n_{OO} states exist, contributing to the ν_{OH} spectrum line width.[86] However, according to the calculated transition moments for the potentials we employ, the ν_{OH} absorbance maximum is dominated by the $n_{OH} = 0$ to $n_{OH} = 1$ transition with $n_{OO} = 0$ in each proton vibrational state, and we will use this transition throughout this work.

3.2. Solvent Dependence of the Proton Stretch Frequency: Polar Solvents. We now characterize the solvent polarity dependence of the proton stretch absorption frequency ν_{AH} in the H-bonded complex in a polar solvent, which is now given by eq 31, via its derivative with respect to $1/\varepsilon$, the inverse of the solvent static dielectric constant. Because the optical dielectric constant ε_∞ for most polar solvents is fairly close to 2,[51,52] we can regard ε_∞ (and thus, the electronic polarization force constant K_∞, eq 9) as constant, so that this derivative can be effected for polar solvents by differentiating eq 31 with respect to the orientational polarization force constant K, eq 14.

Differentiation of our fundamental eq 31 with respect to K gives, again with the aid of the Hellman−Feynman theorem,

$$\frac{dh\nu_{AH}}{dK} = \frac{d\mathcal{E}_1(s_{eq0})}{dK} - \frac{d\mathcal{E}_0(s_{eq0})}{dK} = \langle\phi_0(q, Q, s_{eq0})\left|\frac{dG(q, Q, s_{eq0})}{dK}\right|\phi_0(q, Q, s_{eq0})\rangle - \langle\phi_1(q, Q, s_{eq0})\left|\frac{dG(q, Q, s_{eq0})}{dK}\right|\phi_1(q, Q, s_{eq0})\rangle \quad (32)$$

Noting via eqs 19 and 20 and the equilibrium version of the reaction field eq 16

$$\mathcal{R}_{eq0} = K(\tilde{\mu}_N + s_{eq0}(\tilde{\mu}_I - \tilde{\mu}_N)) \quad (33)$$

that G in eq 32 depends on K both explicitly and via s_{eq0} in $\mathcal{R}_{eq0}$, the G derivative with respect to K can be evaluated via

$$\frac{dG(q, Q, s_{eq0})}{dK} = \frac{\partial G(q, Q, s_{eq0})}{\partial K} + \frac{dG}{d\mathcal{R}}\bigg|_{eq0}\frac{d\mathcal{R}_{eq0}}{dK} \quad (34)$$

With the eq A.1 (Appendix A) expression for G, the first partial derivative is just

$$\frac{\partial G(q, Q, s_{eq})}{\partial K} = -\frac{\mathcal{R}_{eq0}^2}{2K^2} \quad (35)$$

For the $\mathcal{R}_{eq0}$ derivative term, we use the equilibrium version of eq A.5

$$\frac{dG}{d\mathcal{R}}\bigg|_{eq0}\frac{d\mathcal{R}_{eq0}}{dK} = \left[\frac{\mathcal{R}_{eq0}}{K} - \mu(q, Q, s_{eq0})\right]\frac{d\mathcal{R}_{eq0}}{dK} \quad (36)$$

The last three equations then yield

$$\frac{dG(q, Q, s_{eq0})}{dK} = -\frac{\mathcal{R}_{eq0}^2}{2K^2} + \left[\frac{\mathcal{R}_{eq0}}{K} - \mu(q, Q, s_{eq0})\right]\frac{d\mathcal{R}_{eq0}}{dK} \quad (37)$$

which gives the simple result for eq 32

$$\frac{dh\nu_{AH}}{dK} = [\langle\mu\rangle_{eq0} - \langle\mu\rangle_{eq1}]\frac{d\mathcal{R}_{eq0}}{dK} \quad (38)$$

Converting this derivative to one with respect to $1/\varepsilon$ produces a key result of this paper[87−90]

$$\frac{dh\nu_{AH}}{d(1/\varepsilon)} = [\langle\mu\rangle_{eq0} - \langle\mu\rangle_{eq1}]\frac{d\mathcal{R}_{eq0}}{d(1/\varepsilon)} \quad (39)$$

3.3. Solvent Dependence of the Proton Stretch Frequency: Nonpolar Solvents. As already noted in the Introduction, the nonpolar solvent case is much simpler than the situation for polar solvents. This is due to the absence of orientational polarization, so that $\varepsilon = \varepsilon_\infty$ is determined solely by the electronic polarization. There is then no longer any need

dx.doi.org/10.1021/jp501815j | J. Phys. Chem. B 2014, 118, 8330−8351

for the independent solvent coordinate s (cf. eq 16). Indeed, because the orientational polarization force constant K (eq 14) now vanishes, there is no longer any orientational reaction field, $\mathcal{R}(s)$ (eq 16), leaving only K_∞ (eq 9) as the solvent dielectric property in the free energy (eqs 19 and 20).

Thus, the relevant differention of eq 31 for nonpolar solvents is with respect to K_∞ and is directly analogous to eq 32, $h\nu_{AH} = \mathcal{E}_1 - \mathcal{E}_0 = G_1 - G_0$;

$$\frac{dh\nu_{AH}}{dK_\infty} = \frac{d\mathcal{E}_1}{dK_\infty} - \frac{d\mathcal{E}_0}{dK_\infty} = \langle \phi_0(q, Q) \left| \frac{dG(q, Q)}{dK_\infty} \right| \phi_0(q, Q) \rangle - \langle \phi_1(q, Q) \left| \frac{dG(q, Q)}{dK_\infty} \right| \phi_1(q, Q) \rangle \tag{40}$$

With the simplifications just alluded to, the free energy derivative in eq 40 is just

$$\frac{dG(q, Q)}{dK_\infty} = -\frac{1}{2} M_2(q, Q) \tag{41}$$

where M_2 is the square of the electronic dipole moment operator evaluated in the ground electronic state of the complex

$$M_2(q, Q) \equiv \langle \hat{\mu}^2 \rangle_{el} = \mu_N^2(q, Q) c_N^2(q, Q) + \mu_I^2(q, Q) c_I^2(q, Q) \tag{42}$$

involving the dipole moments in, and the populations of, the neutral (N: AH···B) and ionic (I: A^-···HB^+) VB states. (These populations are now given by the nonpolar solvent limit of eq 21 and of course are independent of any solvent coordinate, which has disappeared in this case.)

The theory's predicted slope for nonpolar solvents is simply expressed

$$\frac{dh\nu_{AH}}{dK_\infty} = -\frac{1}{2}\{\langle M_2(q, Q)\rangle_{eq1} - \langle M_2(q, Q)\rangle_{eq0}\} \tag{43}$$

in terms of the difference of M_2 evaluated for the first excited and ground proton stretch vibrational states. This derivative is trivially converted to one with respect to $1/\varepsilon$ via eq 9 with $\varepsilon = \varepsilon_\infty$, yielding another key result of this work, now for nonpolar solvents

$$\frac{dh\nu_{AH}}{d(1/\varepsilon)} = M_S\{\langle M_2(q, Q)\rangle_{eq1} - \langle M_2(q, Q)\rangle_{eq0}\} \tag{44}$$

4. ELABORATION OF THEORETICAL MODEL INGREDIENTS

The theory developed in sections 2 and 3 involves several ingredients, including various structural and free energy properties, that require evaluation for explicit prediction of the ε dependence of the proton frequency ν_{AH} via eqs 39 and 44. But even before numerical estimation can be effected, many of the model ingredients require elaboration, for example, the H-bonded complex dipole moment first needs to be expressed in a form suitable for evaluation. In this section, we discuss the elaboration of a number of these ingredients; some numerical evaluation is included, but much of the numerical parametrization will be outlined in section 4.4. The reader interested primarily in the results of the theory and their explication could proceed directly to section 5.

We begin with details of the quantum chemistry methods employed to obtain the equilibrium H-bonded complex structures, which will provide key structural and charge information (e.g., H-bond lengths and dipole moments) to be employed subsequently. We then describe a simple molecular model for the H-bonded complex's dipole moment μ and its VB state components, μ_N and μ_I. An explicit description of the forms and parametrization of the VB vacuum diabatic potentials, V_N and V_I, then follows. An outline of the overall VB potential parametrization procedure applied to Figure 1 systems is presented in section 4.4.

Before proceeding, we need to introduce an important simplification in some of the calculations. While the polar solvent theoretical formalism presented in previous sections was derived for any ε value, we will use $\varepsilon = \varepsilon_\infty = 2$ (most relevant polar solvents have ε_∞ values fairly close to 2[51,52]) as a reference solvent point to evaluate a number of H-bonded complex properties, including Q_{eq0} and especially the diabatic dipole moments, μ_N and μ_I. From this point forward, all polar solvent variation will involve varying ε, while keeping $\varepsilon_\infty = 2$ fixed; hereafter, this $\varepsilon = \varepsilon_\infty = 2$ reference solvent is the $K = 0$ limit of the polar solvents. When we discus nonpolar solvents with varying $\varepsilon = \varepsilon_\infty$, this reference solvent is simply one particular case $\varepsilon = \varepsilon_\infty = 2$. From here on, we simply term this reference solvent as the "$\varepsilon_\infty = 2$ solvent".

As will be described within, μ_N and μ_I are evaluated only for the $\varepsilon_\infty = 2$ solvent and are thus assumed to be independent of any variation in ε_∞ for both nonpolar and polar solvents and of any orientational polarization contribution to the dielectric constant. This should be a mild approximation, related in part to the fact that this reference solvent already accounts for a significant portion of the solvent polarization effect on these quantities, even for polar solvents. We stress that this $\varepsilon_\infty = 2$ approximation still leaves the significant polar solvent orientational polarization influence on the average dipole moment through the VB state coefficients (e.g., eq 6). Further, because the solvent electronic polarization is equilibrated to the solute electronic structure (as noted in section 2.2), equilibrium solvation H-bond structure calculations are valid for the $\varepsilon = \varepsilon_\infty = 2$ reference equilibrium solvent; this feature allows a straightforward implementation of electronic structure methods in an equilibrated solvent, described next.

4.1. Equilibrium H-Bonded Complex Structures. We employ dielectric continuum electronic structure calculations for the evaluation of several equilibrium H-bonded complex properties. Our goal here is not an accurate calculation of, for example, equilibrium H-bond geometries. This is a daunting task because many configurations occur in equilibrium, and both solvent and H-bonded complex dynamics contribute to the H-bond mode.[47] As stressed in the Introduction, the H-bond pairs and solvents have been chosen such that a fairly stable 1:1 acid−base complex is formed. Our goal is thus to obtain an H-bond geometry that is a fair representative of that stable equilibrium complex, from which the IR absorption maximum is determined. Dynamical fluctuations about this representative complex only contribute to the line-width about that maximum.[47−50]

The procedure begins with an optimization of each of the three isolated acid−DMSO complexes in Figure 1 at the B3LYP/6-311+G** level of theory[91,92] and basis set.[93] The ethanol−DMSO and phenol−DMSO complex geometries were

dx.doi.org/10.1021/jp501815j | J. Phys. Chem. B 2014, 118, 8330−8351

optimized in C_S symmetry, with the two H-bond oxygens, the shared proton, and the DMSO sulfur contained within the symmetry plane. The C_S symmetry is not important for the ethanol−DMSO complex, but it is important for the phenol−DMSO complex, which has two possible orientations with this symmetry. The two configurations for the $\varepsilon_\infty = 2$ equilibrium solvated phenol−DMSO complexes are displayed in Figure 4:

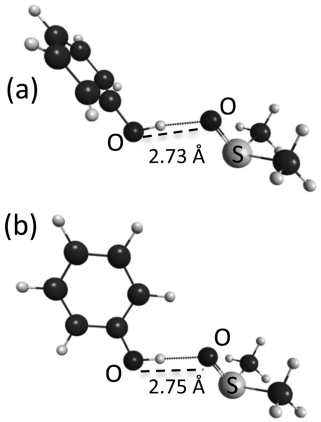

Figure 4. (a) Perpendicular and (b) parallel solvated equilibrium configurations for the phenol−DMSO complex with C_S symmetry and reference solvent dielectric constant $\varepsilon = \varepsilon_\infty = 2$. Equilibrium H-bond lengths are indicated.

the H-bond axis either within the ring plane (the parallel geometry) or primarily perpendicular to the ring plane (the perpendicular geometry). While other gas phase minima exist, these two configurations give fairly linear complexes with the only direct acid−base interaction involving the H-bond, and we take them as reasonable representations of the likely dynamical fluctuations retaining the intact H-bond in the phenol−DMSO complex.[94] The 2-naphthol−DMSO complex is designed in a similar manner in that the complex is optimized with the aromatic rings in the same plane as the H-bond atoms (i.e., the parallel geometry) and primarily perpendicular to the H-bond axis (i.e., the perpendicular geometry).

Finally, we focus on extracting equilibrium H-bond lengths $Q_{eq\infty}$ of the complexes immersed in the reference $\varepsilon_\infty = 2$ solvent, leaving other properties for later subsections. These were obtained by first optimizing the isolated complexes with different fixed Q values, constraining the relative acid−base orientation. Each complex was then immersed in the dielectric continuum $\varepsilon_\infty = 2$ solvent (represented here by cyclohexane), using the Polarizable Continuum Model (PCM)[95] implemented in GAMESS.[96] $Q_{eq\infty}$ is then determined from the complex with the lowest free energy as a function of Q.

The solvated equilibrium ethanol−DMSO structure is depicted in Figure 5, where $Q_{eq\infty} = 2.82$ Å. The two equilibrium solvated phenol−DMSO complexes are shown in Figure 4; their different H-bond lengths (2.73 and 2.75 Å) suggest the level of variation that different complex structures would contribute to the width of the complex's solution phase distribution of H-bond separations. The solvated equilibrium 2-naphthol−DMSO complex perpendicular and parallel geometry complexes shown in Figure 6 are similar to those in Figure 4, including the feature that the perpendicular $Q_{eq\infty}$ is less than the parallel $Q_{eq\infty}$, ∼2.73 and ∼2.74 Å, respectively. Table 2 displays all the $Q_{eq\infty}$ values, with the average listed for the perpendicular and parallel aromatic complexes.

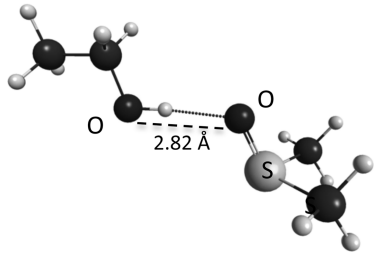

Figure 5. Solvated equilibrium configuration for the ethanol−DMSO complex with C_S symmetry and reference solvent dielectric constant $\varepsilon = \varepsilon_\infty = 2$; the equilibrium H-bond length indicated.

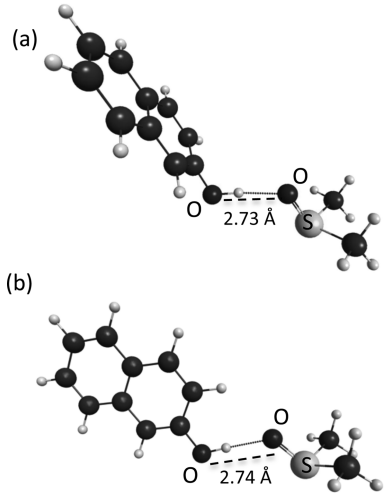

Figure 6. (a) Perpendicular and (b) parallel equilibrium configurations for the 2-naphthol−DMSO complex with reference solvent dielectric constant $\varepsilon = \varepsilon_\infty = 2$; equilibrium H-bond lengths are indicated.

4.2. H-Bonded Complex Dipole Moment Model. We next use the electronic structure calculations to estimate the H-bonded complex dipole moment μ in the reference $\varepsilon_\infty = 2$ solvent. To this end, we first need to describe the simple molecular description for μ that we use to evaluate the H-bonded complex-solvent interaction.

The complex's dipole moment μ in eq 5 is expressed in terms of the q,Q and s-dependent VB state occupations and diabatic dipole moments $\mu_{N,I}$, and we require the q and Q dependence of those moments. For this, we adopt a linear model,[63,97]

$$\mu_N(q) = \mu_{N,o} + a_H(q - q_N);$$
$$\mu_I(q, Q) = \mu_{I,o} + a_H(q - q_I) + a_Q(Q - Q_I) \quad (45)$$

where the coefficients a_H and a_Q describe the diabatic dipole moments' variation with respect to the nuclear coordinates. a_Q will be associated below with the charge transfer component of the ionic state's dipole moment. The reference lengths $q_{N,I}$ in eq 45 are the quantum-average proton positions for each diabatic state, which from the VB potentials presented in the next subsection are always ∼1 Å (within 1%) away from the proton-donor or -acceptor. This criterion then specifies that $q_N = q_o$ and $q_I = Q_I - q_o$, where $q_o = 1$ Å. Q_I here and in eq 45 is defined as the ionic state's ground vibrational equilibrium H-bond length in the reference $\varepsilon_\infty = 2$ solvent. Q_I is approximately the same, ∼2.5 Å, for all three complexes whose ionic state A···B interaction potentials are fairly similar.

dx.doi.org/10.1021/jp501815j | J. Phys. Chem. B 2014, 118, 8330−8351

Table 2. Equilibrium H-Bonded Complex Parameters with Solvation by the Reference $\epsilon = \epsilon_\infty = 2$ Solvent

	$Q_{eq\infty}$ (Å)[a]	$\mu_{N,o}$ (D)[b]	$\mu_{I,o}$ (D)[b]	a_H (e/Å)	a_Q (e/Å)	M_S (kcal/(mol/D^2))[c]
ethanol−DMSO	2.82	6.7	17.5	0.75	0.75	0.053
phenol−DMSO	2.74	8.0	18.2	1.00	0.65	0.086
2-naphthol−DMSO	2.74	8.5	19.5	1.1	0.70	0.056

[a]Complex equilibrium H-bond length in the reference $\epsilon = \epsilon_\infty = 2$ solvent. [b]The H-bonded complex dipole moments for the neutral and ionic VB states are $\mu_{N,o}$ and $\mu_{I,o}$, respectively. See section 4.2 and eqs 45 and 46 for details. [c]M_S values obtained from Figure 1 (see section 4.4 for details).

The reference diabatic dipole moments $\mu_{N,Io}$ in eq 45 are to be determined in the reference $\epsilon_\infty = 2$ solvent[98] and will be identified presently from the quantum chemistry calculations, after certain needed relations are established. From the above definitions, these reference moments are the quantum averages of the diabatic dipole moment expressions (eq 45) evaluated for the ground vibrational state in the respective VB state. With this equation and the parameter definitions above, the ionic reference dipole $\mu_{I,o}$ is just $\mu_{N,o}$ plus two contributions, namely the change in dipole associated with the proton's displacement from q_N to q_I ($q_I = Q_I - q_o$) and a corresponding dipole change over the H-bond length of the ionic state Q_I:

$$\mu_{I,o} = \mu_{N,o} + a_H(Q_I - 2q_o) + a_Q Q_I \quad (46)$$

The difference in eq 45 diabatic dipole moments then depends solely on Q,

$$\mu_I - \mu_N = a_Q Q \quad (47)$$

which establishes the association mentioned below eq 45 that a_Q is associated with the charge transfer over the A−B separation. Equation 5 for $\mu(q,Q,s)$ now takes the form

$$\mu(q, Q, s) = \mu_{N,o} + a_H(q - q_o) + a_Q Q c_I^2(q, Q, s) \quad (48)$$

leaving three parameters $\mu_{N,o}$, a_H, and a_Q (q_o =1 Å), now determined from quantum chemical dipole moment calculations of the section 4.1 equilibrium $\epsilon_\infty = 2$ solvent complexes.

4.2.1. Parametrization. We begin with some strategic considerations for the parametrizations required for the dipole moment. With the same basis set and level of theory used for the section 4.1 PCM calculations, a $\mu(q,Q_{eq\infty})$ curve for each complex is generated by varying the proton position within a complex at certain fixed donor−acceptor separations, $Q_{eq\infty}$ in the $\epsilon_\infty = 2$ solvent. Because K is equal to 0 for the $\epsilon_\infty = 2$ solvent, c_I^2 and μ are s-independent (cf. eqs 19−21).

Figure 7 displays the $\mu(q,Q_{eq\infty})$ curves in the proton coordinate q obtained from the quantum chemistry calculations for each of the three complexes, as well as those generated with the theoretical model eq 48. The curves are sigmoidal with an initial linear region, which mirrors the ionic state population c_I^2 that shifts from 0 at small q to 1 for q near the acceptor B.[36,37] Because PT for the present complexes is quite endergonic with the proton fairly localized with the donor, only the $\mu(q)$ curve's initial part needs to be reasonably represented; thus, only $\mu_{N,o}$ and a_H need to be fairly accurate (for simplicity, we suppress $Q_{eq\infty}$ in the notation in this discussion). These two parameters can be first determined from the initial linear $\mu(q)$ behavior in Figure 7. The remaining parameter a_Q can then be estimated from the ionic contribution to $\mu(q)$ that is significant for q near the acceptor B. We now turn to the details of all this.

We begin with the $\mu_{N,o}$ parametrization; while this and its ionic state analogue are, in principle, quantum-averaged (see discussion above eq 46), this quantization can be neglected here without any important numerical impact.[99] Because, as noted above, full PT is too endergonic to occur for the present complexes in the $\epsilon_\infty = 2$ solvent, each equilibrium structure with $q_{eq} \sim 1$ Å primarily, although not exclusively, reflects the complex's neutral VB state charge distribution. These are the dipole moments near $q \sim 1$ Å in Figure 7,[99] so that $\mu_{N,o}$ is thus defined as the dipole moment of these equilibrium structures, which we modify by a correction removing any charge transfer, ensuring that AH and B are each neutral. We take the $\mu_{N,o}$ values for the phenol− and 2-napthol-DMSO complexes as averages of the perpendicular and parallel configurations (Figure 7).[99] The parametrized $\mu_{N,o}$ values obtained for the three complexes are given in Table 2.

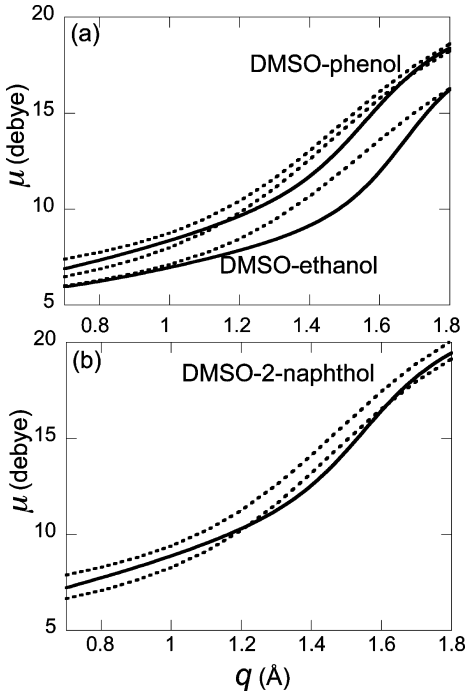

Figure 7. H-bonded complex dipole moment μ versus the proton coordinate q for the H-bond coordinate value $Q = Q_{eq\infty}$ for the (a) ethanol−, phenol−, and (b) 2-naphthol−DMSO complexes with reference solvent dielectric constant $\epsilon = \epsilon_\infty = 2$. Dotted lines indicate quantum chemistry calculations; two sets are present for the aromatic complexes' perpendicular and parallel configurations. Solid lines present the eq 5 theoretical description.

We now turn to the coefficients a_H and a_Q in eq 45. From eq 48, the initial slope of $\mu(q)$ with respect to q is predominantly given by a_H, with an additional contribution from the initial c_I^2 slope. Each complex's a_H value can be determined by matching the theoretical model's initial slope to the quantum chemistry calculated value (Figure 7). As for a_Q, this determines the contribution from the charge transfer component, as indicated in eq 48. Because a_Q accordingly affects $\mu(q)$ more for q values near the acceptor (i.e., $c_I^2(q)$ closer to 1), we set a_Q to a value

dx.doi.org/10.1021/jp501815j | J. Phys. Chem. B 2014, 118, 8330−8351

Table 3. Calculated Red-Shifts ($\Delta\nu$) from the Experimental Free Vacuum OH Frequency[a] and Related Quantities

	ΔPA (kcal/mol)[b]	$\varepsilon = \varepsilon_\infty = 1$ $\Delta\nu$ (cm^{-1})[c]	$\varepsilon = \varepsilon_\infty = 2$ $\Delta\nu$ (cm^{-1})	$\varepsilon = 80$ $\Delta\nu$ (cm^{-1})	$\Delta\nu(\varepsilon = 2) - \Delta\nu(\varepsilon = 1)$ (cm^{-1})	$\Delta\nu(\varepsilon = 80) - \Delta\nu(\varepsilon = 2)$ (cm^{-1})
ethanol–DMSO	167.0	205	237	263	32	26
phenol–DMSO	138.3	286	390	489	104	99
2-naphthol–DMSO	132.5	342	423	496	79	73

[a]For ethanol, ν = 3676 cm^{-1}; for the aromatic alcohols, ν = 3657 cm^{-1}.[112−122] [b]The vacuum proton affinity difference ΔPA defined in eq 50.[105−109] [c]Vacuum $\varepsilon = \varepsilon_\infty = 1$ limit for the H-bonded complex.[133]

Table 4. Polar Solvent Slope and its Components

	ε	ΔPA (kcal/mol)[a]	$d\nu_{AH}/d(1/\varepsilon)$ numerical[b]	$d\nu_{AH}/d(1/\varepsilon)$ theory[c]	$d\langle\mu\rangle_{eq\,0}/d(1/\varepsilon)$ factor[d]	M_S[e]	$\langle\mu\rangle_{eq\,0}$ (D)	$\Delta\langle\mu\rangle_{10}$ (D)[f]	$\Delta\langle\mu\rangle_{10}\langle q\rangle$ (D)[g]	$\Delta\langle\mu\rangle_{10}$ CT (D)[h]
ethanol– DMSO	2	167.0	52	52	1.0	0.053	6.93	0.20	0.14	0.06
ethanol–DMSO	80	167.0	55	55	1.003	0.053	6.97	0.21	0.14	0.07
phenol–DMSO	2	138.3	188	186	1.0	0.086	8.38	0.37	0.24	0.13
phenol–DMSO	80	138.3	224	227	1.010	0.086	8.45	0.44	0.26	0.18
2-naphthol–DMSO	2	132.5	140	141	1.0	0.056	8.91	0.40	0.26	0.14
2-naphthol–DMSO	80	132.5	160	161	1.007	0.056	8.97	0.46	0.28	0.18

[a]The vacuum proton affinity difference ΔPA defined in eq 50.[105−109] [b]Numerical evaluation of the frequency versus $1/\varepsilon$ slope of Figure 1 theoretical polar solvent data curves (cf. the numerical slope versus $1/\varepsilon$ behavior in Figure 9a for the phenol–DMSO complex). Units: cm^{-1}. [c]The $d\nu_{OH}/d(1/\varepsilon)$ slope evaluated via eq 53. Units: cm^{-1}. [d]The eq 53 factor in curly brackets associated with the derivative $d\langle\mu\rangle_{eq0}/d(1/\varepsilon)$; the closeness of this factor to unity indicates the validity of the simplification leading from eq 53 to the approximate eq 54 for the polar solvent slope. [e]Structure factor M_S values for the theoretical lines in Figure 1; units: kcal/(mol/D^2). [f]The H-bonded complex's dipole moment change in the vibrational transition $\langle\mu\rangle_{eq1} - \langle\mu\rangle_{eq0}$ (cf. in eq 57). [g]OH stretch component of the dipole moment change in the transition of eq 57. [h]The charge transfer component of the dipole moment change in the transition of eq 57.

Table 5. Nonpolar Solvent Slope and Its Components Evaluated at $\varepsilon = \varepsilon_\infty = 2$

	ΔPA[a] (kcal/mol)	M_S[b]	$\langle\mu\rangle_{eq0}$ (D)	$d\nu_{OH}/d(1/\varepsilon)$ numerical[c]	$d\nu_{OH}/d(1/\varepsilon)$ theory[d]	$\Delta\langle\mu_N^2\rangle_{10}$ (D^2)[e]	$\Delta\langle c_I^2\mu_{N,I}^2\rangle_{10}$ (D^2)[f]
ethanol– DMSO	167.0	0.053	6.93	70	70	2.05	1.72
phenol–DMSO	138.3	0.086	8.38	233	233	4.06	3.69
2-naphthol–DMSO	132.5	0.056	8.91	181	181	4.89	4.36

[a]The vacuum proton affinity difference, ΔPA, defined in eq 50.[105−109] [b]M_S values for the theoretical lines in Figure 1; units of M_S are kcal/(mol/D^2). [c]Numerical evaluation of the slope of Figure 1 theoretical nonpolar solvent data. Units are cm^{-1}. [d]The $d\nu_{OH}/(1/\varepsilon)$ nonpolar slope evaluated with eq 58 (equivalent to the sum of the CT and non-CT components of the sixth and seventh columns multiplied by M_S in the second column and the 349.8 cm^{-1} mol/kcal conversion factor). Units are cm^{-1}. [e]The non-CT square brackets term of the first difference in eq 58: $\Delta\langle\mu_N^2\rangle_{10} = (\langle\mu_N^2\rangle_1 - \langle\mu_N^2\rangle_0)$. [f]The CT square brackets term of the second difference in eq 58: $\Delta\langle c_I^2\mu_{N,I}^2\rangle_{10} = [\langle c_I^2(\mu_N^2 - \mu_N^2)\rangle_1 - \langle c_I^2(\mu_N^2 - \mu_N^2)\rangle_0]$.

that gives the correct $\mu(q)$ value for $Q = Q_{eq\infty}$ and $q = q_{Imin} = Q_{eq\infty} - q_o$, that is, the $\mu(q)$ values after the inflection point shown in Figure 7. Because $c_I^2(q)$ is only known after the model's full parametrization including the VB potentials, the final a_H and a_Q coefficients' parametrization is actually effected by iterative determination along with M_S and the VB potential parameters (cf. section 4.4), then verifying that the theory generates reasonable $\mu(q)$ trends (Figure 7). Their values so determined are given in Table 2.[100]

4.3. Valence Bond Potentials. We now turn to the vacuum VB potentials $V_{N,I}$ in the free energy (eq 20) and their various components. Our focus here is on the structure and significance of these potentials. Their details and parametrization are largely relegated to Appendix B.

Each potential $V_{N,I}$ comprises three nuclear coordinate-dependent parts, as in previous work:[36,37,39,62,104]

$$V_N(q, Q) = V_{AH}(q) + V_{nHB}(Q - q) + V_{N,AB}(Q);$$
$$V_I(q, Q) = V_{HB+}(Q - q) + V_{nAH}(q) + V_{I,AB}(Q) + \Delta_{vac} \quad (49)$$

The ionic VB potential V_I contains the gas phase energy offset Δ_{vac} (ionic minus neutral) between the VB potential minima for separated AH and B. This corresponds to the gas phase proton affinity (PA) difference, ΔPA, between the base B and HA's conjugate base A^-

$$\Delta_{vac} = \Delta PA = PA(A^-) - PA(B) \quad (50)$$

whose H-bonded complex values are presented in Tables 3–5.[105−109] V_{AH} and V_{HB+} in eq 49 are the vacuum proton donor AH and HB^+ protonated acceptor proton stretch potentials, described by Morse potentials (see eq B.1), with parameters consistent with the bond dissociation energy[110] and OH stretch frequencies (ν_{AH} = 3676 cm^{-1} for ethanol[105−111] and ν_{AH} = 3657 cm^{-1} for the phenol and 2-naphthol aromatic acids;[111−122] Table 6). The protonated DMSO HB^+ frequency value is taken to be similar to that for H_3O^+ with $\nu_{HB+} \approx$ 3700 cm^{-1}.[123,124]

The nonbonded interactions V_{nHB} and V_{nAH} in eq 49 involve electrostatic and van der Waals interactions between the proton and the nonbonded nuclei.[39,104] As in previous work,[104] the neutral state nonbonding interaction V_{nHB} is primarily modeled by a Morse potential (see eq B.2). For the ionic state V_{nAH} potential, an extra electrostatic interaction is added to this V_{nAH} Morse potential because the donor now has a net negative charge (see eq B.3). As will be discussed in section 4.4, the nonbonding Morse parameters for V_{nHB} and V_{nAH} are determined by ensuring an appropriate H-bonded complex frequency ν_{AH} in the ε_∞ = 2 solvent.

dx.doi.org/10.1021/jp501815j | J. Phys. Chem. B 2014, 118, 8330−8351

Table 6. Proton Vibrational Stretch V_{AH} and V_{HB+} Morse Parameters of Equation B.1

	D_{OH} (kcal/mol)	a_{OH} (Å^{-1})	r_{OH} (Å)
ethanol[a]	110.0	2.41	0.96
phenol[b]	95.0	2.60	0.96
2-naphthol[b]	95.0	2.60	0.96
DMSOH^{+}[c]	145.3	2.08	0.97

[a]The isolated molecule stretch frequency for ethanol, ν_{AH} = 3676 cm^{-1}.[111−122] [b]For the phenol and 2-naphthol aromatic acids, ν_{AH} = 3657 cm^{-1}.[111−122] [c]For protonated DMSO, $\nu_{HB+} \approx$ 3700 cm^{-1}.[123,124]

The final coordinate−dependent contributions $V_{N,AB}$ and $V_{I,AB}$ in eq 49 are associated with the H-bond mode (i.e., the A···B interaction). For the neutral state, $V_{N,AB}$ is also taken as a Morse potential (eq B.4). In the ionic state, the H-bond interaction $V_{I,AB}$ includes an extra electrostatic term corresponding to the attraction between positively charged B and negatively charged A. This interaction is similar for the three H-bonded complexes (eq B.5), with the Coulomb coefficient, C_{Qelec}, estimated by a H-bonded complex vacuum calculation. The $V_{N,AB}$ and $V_{I,AB}$ Morse parameters listed in Table 7 were determined by ensuring an appropriate equilibrium H-bond separation and frequency ν_Q for the ε_∞ = 2 solvent H-bonded complex, whose geometry was discussed in section 4.1.

Finally, the electronic coupling β in eq 19 is taken as an exponential function in the H-bond separation

$$\beta(Q) = \beta_o \exp[-\alpha_e Q] \tag{51}$$

Parameters are similar to those used previously for OH···O complexes,[34,36,37,62] β_o = −1604 kcal/mol and α_e = 1.5 Å^{-1}, and appropriately yield β values on the order of 1 eV for the present equilibrium H-bonded complex separations.

4.4. Parametrization. Most of the parameters, including the proton affinity difference ΔPA (Table 3−5), the reference diabatic VB dipole moments $\mu_{N,o}$ and $\mu_{I,o}$ (Table 2), and the Morse parameters for the free AH and HB$^+$ stretches (eq B.1 and Table 6), are defined a priori via vacuum experimental measurements or quantum chemistry. We have already discussed aspects of the parametrization for geometries and dipole moment quantities earlier in this section. It remains to determine the Morse parameters for the nonbonding interactions (eqs B.2 and B.3) and the A···B interaction (eqs B.4 and B.5), as well as the structure factor M_S (Tables 2 and 5). We emphasize again the importance of the particular nonpolar $\varepsilon = \varepsilon_\infty$ = 2 solvent as a reference point. Now we need to go slightly beyond this, while retaining the emphasis on parametrization via a nonpolar solvent perspective, allowing independent prediction for polar solvents via the theory. In particular, we will iteratively optimize both the nonbonding interaction parameters and M_S to obtain the correct ν_{AH} magnitude for the ε_∞ = 2 solvent and another nonpolar solvent with $\varepsilon = \varepsilon_\infty$ = 2.5.

We start with the H-bond vibration's Morse parameters. Many (∼15) H-bond vibrational levels need to be quantized in order to access the first excited proton stretch level. Because the first excited proton stretch level lies ∼9 kcal/mol above the zero point level, this causes certain problems with the simultaneous (q, Q) quantization that we employ when the A···B interaction well depth D_{OO} (eqs B.4 and B.5) has a reasonable value for the given complexes, related to the presence of a continuum of H-bond vibrational states. To finesse this problem, the well depth D_{OO} was set for all the complexes to 9 kcal/mol. We hasten to add that this artificial maneuver, together with other adjustments to the H-bond potential, nonetheless enables the simultaneous generation of correct proton frequencies ν_{AH} and physically reasonable values of the relevant H-bond parameters for the problem; it is not used to incorrectly predict that the dissociation energies or free energies are the same and so large for each complex. With the well depth set in this fashion, the H-bond frequency ν_Q is set to be ∼200 cm^{-1}[1126] via adjustment of the exponential parameter a_{OO}, shown in Table 7, while the equilibrium H-bond separation $Q_{eq\infty}$ is set by the well's minimum position r_{OO} (eqs B.4 and B.5).[126,127]

We now turn to the nonbonding Morse parameters (eqs B.2 and B.3). First, r_{nOH} was set to a value (1.2 Å) larger than the OH bond length (∼1 Å), consistent with a weak nonbonding interaction. Next, a_{nOH} is set to the OH exponential parameter a_{OH} in Table 2, except for the ethanol−DMSO complex, for which a_{nOH} is set slightly less than a_{OH} to ensure that $\nu_Q \sim 200$ cm^{-1}; the nonbonding potential and, in particular, a_{nOH} contribute to the H-bond potential's attractive portion, and a larger a_{nOH} value would yield a significantly higher ν_Q.

With the above H-bond vibration's parameters, only the nonbonding well depth D_{nOH} and the structure factor M_S remain to be determined. Because both the ν_{AH} magnitude and the nonpolar solvent slope versus $1/\varepsilon$ for the ε_∞ = 2 solvent depend on both D_{nOH} and M_S, these parameters are iteratively varied to obtain the correct values of these two items. Their specific parametrization using the available experimental Figure 1 nonpolar solvent data involves the following. This data versus $1/\varepsilon$ is first fit to a line, and two target frequencies for ε = 2 and 2.5 are taken from this line. The two parameters, D_{nOH} and M_S, are then varied to match these two target ν_{OH} values (within ∼1 cm^{-1}) evaluated using the theoretical model for nonpolar solvents with $\varepsilon = \varepsilon_\infty$. The resulting M_S and D_{nOH} values are listed in Tables 2 and 7, respectively.

The structure factor M_S is studied further in the Supporting Information to confirm that it is ε-independent and its parametrization presented here is reasonable. Its characteristics useful for the interpretation of the theory's application in section 5 are also presented. Further, aspects of the M_S parametrization are discussed, which indicate that caution in the interpretation of detailed trends for M_S is called for; such interpretation should be reliable within families of complexes

Table 7. Nonbonding and O···O Interaction Morse Parameters of Equations B.2−B.5

	D_{nOH} (kcal/mol)	a_{nOH} (Å^{-1})	r_{nOH} (Å)	D_{OO} (kcal/mol)	a_{OO} (Å^{-1})	r_{OO} (Å)	m_Q (amu)[a]	C_{Qelec}[b]
ethanol−DMSO	13.4	2.0	1.20	9.0	1.8	3.04	19	1.3
phenol−DMSO	9.5	2.6	1.20	9.0	2.5	2.89	43	1.1
l2-naphthol−DMSO	12.1	2.6	1.20	9.0	2.5	2.89	51	1.0

[a]The reduced mass of the acid−base dimer: $m_Q = (m_{AH}\, m_B)/(m_{AH} + m_B)$. [b]The coefficient in the extra H-bond donor−acceptor electrostatic interaction in the ionic VB state, C_{Qelec}, is defined in eq B.5.

dx.doi.org/10.1021/jp501815j | J. Phys. Chem. B 2014, 118, 8330−8351

(e.g., aromatic), but may not be when comparing families (e.g., aliphatic and aromatic) (section Sb.1, Supporting Information).

5. ANALYSIS OF THE ν_{AH} MAGNITUDE AND VARIATION WITH SOLVENT

With the parametrization for the theory completed, we can now turn to the theoretical results successfully compared to those of experiment in Figure 1 for the proton frequencies $\nu_{AH} = \nu_{OH}$ for the three H-bonded complexes in polar and nonpolar solvents. (We retain the ν_{AH} notation for ease of referring to previous results in the paper). We first describe how Figure 1 theoretical curves are generated. Then, after some general remarks concerning the results, we discuss some key determining sources of the ν_{OH} magnitudes, for example, H-bond formation, proton affinity difference between the H-bond donor and acceptor, solvent electronic polarization, and solvent orientational polarization. Next, after verifying the validity of the two theoretical slope expressions (eqs 39 and 44) for the frequency change with inverse solvent dielectric constant, we employ them to analyze Figure 1 frequency curves via their slopes, in terms of the influence of, for example, the H-bonded complex size, dipole moment, and dipole moment change and charge transfer in the vibrational transition.

5.1. Theory Application for Figure 1. *5.1.1. Polar Solvents.* We discuss Figure 1 polar solvents first. For a given H-bonded complex and solvent, the desired proton vibrational frequency ν_{AH} is given by eq 31, the energy gap between the ground and first excited proton stretch eigenlevels (Figure 3). This requires the ground and excited vibrational state quantum averages $G_0(s)$ and $G_1(s)$ of the free energy $G(q,Q,s)$ eq 19, whose ingredients are all defined in section 2, with the required parametrizations described in section 4. (Recall that predictions for polar solvents are made with *no* further parametrization.) For a given solvent dielectric constant ε, each of these averages is to be evaluated at the ground state equilibrium solvent coordinate, s_{eq0}, defined by the $G_0(s)$ minimization condition (eq 28, Figure 2b). All this is implemented as follows.

The vibrational state free energies $G_0(s)$ and $G_1(s)$ for quantized proton and H-bond coordinates are computed as the required first step. The free energy vibrational eigenvalues and corresponding wave functions must be obtained for several solvent coordinate s values, via numerically solving the two-dimensional vibrational Schrödinger eq 23 for each s. As in previous PT work,[36,37,39,62] eq 23 is solved using a discrete variable representation basis[128,129] with equally spaced grid points[130] while properly accounting for the kinetic energy coupling for a colinear three-body system.[36,37,39]

The second step is to find the ground state equilibrium solvent coordinate value s_{eq0} by evaluating $G_0(s)$ at a number of solvent coordinate, s, values and finding its minimum, which locates s_{eq0};[131] the $G_1(s_{eq0}) - G_0(s_{eq0})$ energy gap at this point gives the desired frequency ν_{AH} for the given ε value.

Finally, the theoretical polar solvent results in Figure 1 are then generated as a series of ν_{AH} values for a given H-bonded complex by inputting a series of ε values between 2 and 80 into the theoretical model just described with $\varepsilon_\infty = 2$ constant. Here, $\varepsilon = \varepsilon_\infty = 2$ is obviously the lower nonpolar solvent limit because for any smaller ε the polar solvent force constant eq 14 K would be unphysically negative.

As noted in the Introduction, the theory's agreement with the experimental polar solvent data is quite satisfactory. We will return to a slightly more refined version, which takes into account that the ε_∞ value for polar solvents is not exactly 2, after we deal with nonpolar solvents.

5.1.2. Nonpolar Solvents. For nonpolar solvents, the generation of the frequency curves in Figure 1 from the theoretical eq 40 (first member) is more straightforward than for polar solvents because s-minimization is not required. There is no orientational polarization factor or reaction field and no solvent coordinate, as explained in section 3.3. Thus, G_0 (as well as G_1 in the nonpolar solvent frequency eq 40) is s-independent, as is the underlying full free energy eq 19, now taken in its $s = 0$ form $G(q,Q,s = 0)$.

For a given H-bonded complex, the nonpolar solvent frequencies are calculated for a series of $\varepsilon = \varepsilon_\infty$ values between 1.5 and 3.[132] The agreement with the experimental nonpolar solvent frequency values in Figure 1 is quite good, but of course, this is strongly assisted by our parametrization described in section 4.4 for nonpolar solvents.

Above, we have treated the polar solvents under the simplifying assumption that each one has a fixed $\varepsilon_\infty = 2$ value; this allows a slope to be easily characterized. But ε_∞ differs slightly from 2 for the various polar solvents. The theory just as described in section 5.1.1, but without the $\varepsilon_\infty = 2$ assumption, can be used to evaluate ν_{AH} for any ε and ε_∞ pair solvent by simply using the appropriate two dielectric constants for each solvent; the nonpolar solvent limit is automatically recovered if $\varepsilon = \varepsilon_\infty$. Figure 8 displays the resulting theoretical

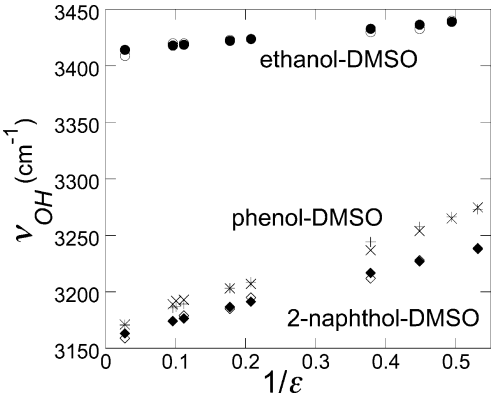

Figure 8. Theoretical OH vibrational stretch frequency $\nu_{AH} = \nu_{OH}$ for each Figure 1 solvent, calculated from the full theory with appropriate solvent static and high frequency dielectric constant values (ε, ε_∞) for each solvent, as described in section 5.1, and the corresponding experimental ν_{OH} data versus $1/\varepsilon$ for ethanol−DMSO (○, ●), phenol−DMSO (×, +), and 2-naphthol−DMSO (◇, ◆) complexes. The first symbols (○, ×, ◇) denote experimental points, while the second symbols (●, +, ◆) denote theoretical points. Solvents from lowest ε to highest ε are hexane, cyclohexane, CCl_4, CS_2, chloroform, chlorobenzene, dichloromethane, 1,2-dichlorobenzene, 1,2-dichloroethane, and acetonitrile.

predictions and the experimental[18] frequency values. Again, the theory agreement for both solvent types is excellent; but as indicated above, the agreement for the nonpolar solvents is assisted by the nonpolar solvent parametrization in section 4.

5.2. ν_{AH} Magnitude. We now analyze the ν_{AH} magnitudes predicted by the theory to begin to comprehend key contributing features. To this end, we calculate the theoretical ν_{AH} values of Figure 1 H-bonded complexes for three different solvent dielectric constant sets $\varepsilon = \varepsilon_\infty = 1$ and 2, and $\varepsilon = 80$ with $\varepsilon_\infty = 2$ and consider their red-shifts from the experimental vacuum free OH frequency. Table 3 lists these shifts ($\Delta\nu$) and

dx.doi.org/10.1021/jp501815j | J. Phys. Chem. B 2014, 118, 8330−8351

the differences in shifts. The first $\varepsilon = \varepsilon_\infty = 1$ frequency shift from the vacuum assesses the impact of H-bond formation in vacuum. The difference of the frequency shifts for $\varepsilon = \varepsilon_\infty = 2$ and 1 then assesses the contribution of the (reference nonpolar) solvents' electronic polarization, while the final difference of the shifts for $\varepsilon = 80$ and $\varepsilon = \varepsilon_\infty = 2$ reflects the influence of the solvent's orientational polarization when ε is large.

We show in Table 3 that the ordering of the $\varepsilon = \varepsilon_\infty = 1$ "vacuum H-bonded complex formation" shifts[133] from the vacuum OH frequency follows the vacuum proton affinity difference $\Delta PA = PA(A^-) - PA(B)$. Because the base DMSO is common to all three complexes, the ν_{OH} decrease with decreasing ΔPA reflects the increased acidity going from a ethanol to 2-naphthol H-bond donor, a correlation consistent with the frequency red-shift increase accompanying stronger H-bond formation.[1−8]

Next, immersion of the H-bonded complex in a nonpolar solvent with only electronic polarization (i.e., the $\varepsilon_\infty = 2$ solvent) further decreases ν_{OH}, as reflected in the frequency shift difference for $\varepsilon = \varepsilon_\infty = 2$ and 1 (Table 3). This is due to the preferential solvation and increased contribution of the ionic state relative to the neutral state and to a correspondingly smaller H-bond separation Q_{eq0}. Comparison of Table 3 $\varepsilon = \varepsilon_\infty = 1$ and $\varepsilon = \varepsilon_\infty = 2$ $\Delta\nu$ shifts reveals an important point: the vacuum shift due to the H-bonded complex formation is the dominant component of the $\varepsilon = \varepsilon_\infty = 2$ ν_{OH} magnitude because it contributes more than 70% of the $\varepsilon_\infty = 2$ solvent shift. This feature strongly argues against the common use of a dielectric continuum solvation model focused solely on the H-bond donor. This frequency shift difference depends on the two factors that determine the $\varepsilon_\infty = 2$ solvent solvation free energy (cf. eq 8): M_S, that is, the size of the complex, and the complex's dipole moment (we remind the reader of the cautionary remark concerning M_S at the conclusion of section 4.4). This difference is smallest for ethanol−DMSO with the smallest dipole moment (cf. Table 4). The phenol−DMSO complex has the largest difference because it has a larger dipole moment than ethanol−DMSO and is smaller in size than the 2-naphthol−DMSO complex, that is, it has a larger M_S.

Finally, ν_{OH} is further decreased in polar solvents with $\varepsilon > 2$, as (nonequilibrium) orientational polarization enhances the preferential solvation of, and the contribution from, the ionic state relative to the neutral state. Table 3 shows that, for each complex, the two $\Delta\nu$ differences—from the vacuum to $\varepsilon = \varepsilon_\infty = 2$, and from there to $\varepsilon = 80$—are approximately identical. This reflects a near saturation of the influence of the solvent orientational polarization on the frequency, at a value comparable to that of the solvent electronic polarization; note that the corresponding free energetic solvent force constant expressions eqs 14 and 9 are essentially numerically equivalent when $\varepsilon_\infty = 2$ and $\varepsilon = 80$.[134]

5.3. Slope Analysis and Charge Transfer. We now turn from the frequency magnitudes to the description of the slopes in Figure 1 in terms of the polar and nonpolar slope theoretical expressions in eqs 39 and 44, respectively; this will allow a detailed interpretation of the H-bond frequency behavior.

5.3.1. Polar Solvent Slope. We first address Figure 1 slopes starting via analysis of eq 39 polar slope expression. We begin by confirming it numerically, which requires evaluation of the reaction field derivative there. Combining eqs 30 and 33 yields a useful form for $\mathcal{R}_{eq0}$

$$\mathcal{R}_{eq0} = K\langle\mu\rangle_{eq0} \tag{52}$$

such that $d\mathcal{R}_{eq0}/d(1/\varepsilon)$ in eq 39 may be expressed as a function of the equilibrium ground state dipole moment and its derivative:

$$\frac{dh\nu_{AH}}{d(1/\varepsilon)} = 2M_S[\langle\mu\rangle_{eq1} - \langle\mu\rangle_{eq0}]\langle\mu\rangle_{eq0} \left\{1 + \frac{[1/\varepsilon_\infty - 1/\varepsilon]}{\langle\mu\rangle_{eq0}}\frac{d\langle\mu\rangle_{eq0}}{d(1/\varepsilon)}\right\} \tag{53}$$

To check eq 53, we calculate the theoretical polar solvent slope from Figure 1, that is, the numerical derivative of $h\nu_{AH}$ with respect to $1/\varepsilon$ using the phenol−DMSO complex theoretical curve there. The resulting slope, itself plotted versus $1/\varepsilon$, is displayed as the solid line in Figure 9a, which shows that the slope varies somewhat with ε, a point that is also exposed in Table 4 for all the complexes and one to which we return below. The major point for now is that we take this slope as our standard of comparison for our eq 53 because the original theoretical ν_{AH} versus $1/\varepsilon$ curve in Figure 1 is in good agreement with the experimental phenol−DMSO complex data. The result for the slope according to eq 53 is given as the dotted line in Figure 9a. As explained in the Figure 9a caption, this confirms the validity of eq 53 within uncertainties (<2%) related solely to assorted numerical evaluation issues. Because comparable confirmation applies for the other two H-bonded complexes (not shown), we can then take the polar slope eq 53 with confidence as a basis in order to analyze the important contributions to the frequency variation with the polar solvent dielectric constant.

As an aside, we also plot in Figure 9a the approximate expression which ignores μ variation with $1/\varepsilon$ (i.e., setting the argument in eq 53's curly brackets to unity):

$$\frac{dh\nu_{AH}}{d(1/\varepsilon)} \approx 2M_S[\langle\mu\rangle_{eq1} - \langle\mu\rangle_{eq0}]\langle\mu\rangle_{eq0} \tag{54}$$

This simpler polar solvent slope description is clearly a quite good approximation[136] and agrees with the solid line slope within the uncertainties of the latter.

As expected, given the above, each theoretical slope equation provides an excellent description for the frequency ν_{AH} itself, as is shown in Figure 9b via the first line of the integral relation

$$h\nu_{pol}(\varepsilon, \varepsilon_\infty) = h\nu_{AH}(\varepsilon = \varepsilon_\infty = 2) - \int_{1/2}^{1/\varepsilon}\left(\frac{dh\nu_{AH}(\varepsilon, \varepsilon_\infty)}{d(1/\varepsilon)}\right)_{polar} d(1/\varepsilon)$$
$$\approx h\nu_{AH}(\varepsilon = \varepsilon_\infty = 2) + \left(\frac{dh\nu_{AH}(\varepsilon)}{d(1/\varepsilon)}\right)_{polar}\left(\frac{1}{\varepsilon} - \frac{1}{2}\right) \tag{55}$$

where ν_{AH} $(\varepsilon = \varepsilon_\infty = 2)$ is the $\varepsilon = \varepsilon_\infty = 2$ reference solvent's frequency. The second line of eq 55 is the linear limit with a constant polar slope,[137] which is clearly not a good approximation in view of Figure 9a. Nonetheless, we include it (with the $\varepsilon = \varepsilon_\infty = 2$ polar solvent slope value) in Figure 9b to give an indication of both the consequence of the slope variation in Figure 9a and the nonlinearity in ν_{AH}; Figure 9a shows that the effect is noticeable but not dramatic. There is a <10 cm^{-1} effect for the highest solvent polarity $\varepsilon = 80$, which is smaller for the other two complexes 2-naphthol− and ethanol−DMSO, which have a smaller polar solvent slope variation (cf. Table 4).

dx.doi.org/10.1021/jp501815j | J. Phys. Chem. B 2014, 118, 8330−8351

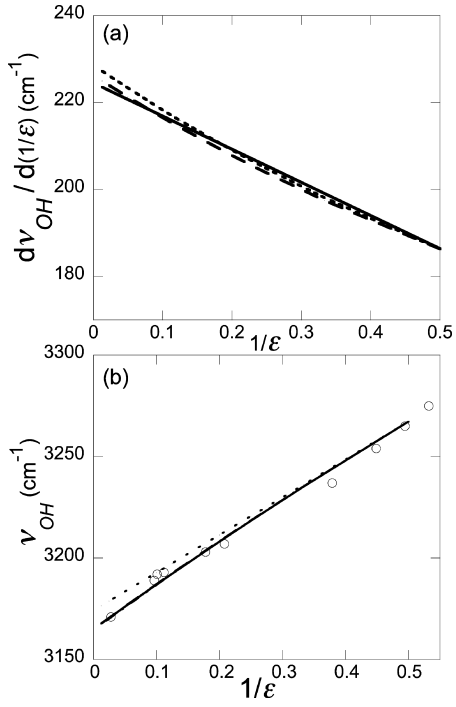

Figure 9. (a) Different evaluations of the slope of $h\nu_{AH} = h\nu_{OH}$ with respect to the inverse of the solvent static dielectric constant $1/\varepsilon$ versus $1/\varepsilon$, for the phenol−DMSO complex in polar solvents. Numerical evaluation of the slope of the theoretical curve in Figure 1 (obtained via a fit of the theoretical ν_{OH} points, computed as in section 5.1, to a polynomial) versus $1/\varepsilon$ (solid line) and the theoretical polar slope expression from eq 53 (dotted line). As stated in the text, these agree within numerical uncertainties (<2%) associated with the evaluations. The uncertainty associated with the first fit and numerical differentiation of the polynomial, combined with the uncertainty involved in evaluating ν_{OH} with the theoretical model, yields an uncertainty for this numerical slope at ∼1%. The eq 53 expression is evaluated with the wave functions obtained from the ν_{OH} evaluation, with an estimated uncertainty for this slope also at ∼1%. Because the slopes in the figure are within <2% of each other, this is within the uncertainty of the slope evaluations. Finally, the approximate eq 54 expression ignoring μ variation with $1/\varepsilon$ is also included (dashed line). (b) The experimental ν_{OH} points for the phenol−DMSO versus $1/\varepsilon$ of Figure 1, the corresponding Figure 1 polar solvent curve (solid line), the integral using eq 54 ν_{OH} polar solvent slope from eq 53 (dashed line), and its approximation from eq 54 (dotted-dashed line). Evaluation of the latter two curve values were afforded with a numerical integration of the respective slope curves in (a). Finally, the linear version of eq 55 with the constant polar slope, evaluated for the reference $\varepsilon_\infty = 2$ solvent, is provided (dotted line). There is a <10 cm^{-1} effect of the constant slope approximation for the highest solvent polarity $\varepsilon = 80$; this is smaller for the other two complexes (2-naphthol− and ethanol−DMSO), which have a smaller polar solvent slope variation, evident from the polar slope difference for $\varepsilon = 2$ and $\varepsilon = 80$ in Table 4.

We now turn to an analysis of the various contributions of Figure 1 polar solvent slopes. To this end, we will use the simplified but still quite accurate eq 54 expression (Figure 9a,b and Table 4); this specifies three contributions: the structure factor M_S (inversely related to the complex's size/geometric aspects), the dipole moment change $\Delta\langle\mu\rangle_{10} = \langle\mu\rangle_{eq1} - \langle\mu\rangle_{eq0}$ in the vibrational transition, and the complex's ground state dipole moment $\langle\mu\rangle_{eq0}$, with all dipole moments being quantum-averaged quantities. These are all collected, for all three H-bonded complexes and two solvent dielectric constant values $\varepsilon = \varepsilon_\infty = 2$ and $\varepsilon = 80$, in Table 4, which also gives information about the slope value itself and the approximate validity of eq 54.

We begin by assessing the source of order of the slope magnitudes for the complexes at any ε value. The ethanol−DMSO complex has the smallest slope by a factor of 3−4 due to its smallest value for all three components (M_S, $\langle\mu\rangle_{eq0}$, and $\Delta\langle\mu\rangle_{10}$). The aromatic complexes have much larger slopes, with the smaller phenol complex having the larger M_S value and slope, despite its slightly smaller, albeit similar, dipole moment and dipole moment change values.

The H-bonded complex's dipole moment change, $\Delta\langle\mu\rangle_{10}$, in the transition is clearly characteristic of the proton vibration. The theory indicates that there are three important aspects to this change: its importance for the variation with solvent dielectric constant, its connection to acid−base properties within the complex, and the occurrence of charge transfer in the vibrational transition, now discussed in turn.

First, Table 4 shows that $\Delta\langle\mu\rangle_{10}$ varies much more percentage-wise with ε than does the equilibrium ground state dipole moment, such that the slope variation in Figure 9a (quantified in Table 4) is clearly dominated by this vibrational transition characteristic. This feature reflects the greater sensitivity to potential anharmonicity (which increases with ε) of $\Delta\langle\mu\rangle_{10}$ compared to $\langle\mu\rangle_{eq0}$, due to the involvement of the larger amplitude excited state vibration. Second, Table 4 shows that $\Delta\langle\mu\rangle_{10}$ correlates with acidity, that is, the difference in eq 50 ΔPA of the proton affinities (PAs) of the proton-accepting base and the conjugate base of the proton-donating acid; because the DMSO base is constant in our complexes, the more acidic the OH proton donor (i.e., the smaller its conjugate base's PA and, here, ΔPA), the greater the proton potential anharmonicity and thus $\Delta\langle\mu\rangle_{10}$.

Third and finally, we can analyze $\Delta\langle\mu\rangle_{10}$ to reveal the importance of charge transfer (CT) in the vibrational transition. For this purpose, we combine dipole moment expression eq 5 with the dipole model eq 45 to give for the nth vibrational state

$$\langle\mu\rangle_{eqn} = \mu_{N,o} + a_H\langle q - q_o\rangle_{eqn} + a_Q\langle Q\rangle_{eqn}\langle c_I^2\rangle_{eqn} \qquad (56)$$

in which the common equilibrium solvent coordinate is that of the proton vibration ground stretch and we made the excellent approximation of splitting the average $\langle c_I^2 Q\rangle_{eqn}$.[138] With eq 56, $\Delta\langle\mu\rangle_{10} = \langle\mu\rangle_{eq1} - \langle\mu\rangle_{eq0}$ is then

$$\Delta\langle\mu\rangle_{10} = a_H(\langle q\rangle_{eq1} - \langle q\rangle_{eq0}) + a_Q(\langle Q\rangle_{eq1}\langle c_I^2\rangle_{eq1} - \langle Q\rangle_{eq0}\langle c_I^2\rangle_{eq0}) \qquad (57)$$

The dipole difference $\Delta\langle\mu\rangle_{10}$ in the vibrational transition has two components. The first, which would be the sole component in models without CT, is associated with the A−H stretch elongation, while the second, which is also explicitly captured by our VB model, is due to CT between the acid and base in the transition, which depends on the quantum-averaged H-bond length Q. Table 4 exhibits both components; each one is positive because the average proton position and the ionic component VB population c_I^2 are larger in the excited state due to the proton potential's anharmonicity. In particular, the $\Delta\langle\mu\rangle_{10}$ CT component in eq 57 is positive despite the fact that $\langle Q\rangle_1$ is less than $\langle Q\rangle_0$ due to an important increase in the complex's ionic character in the excited state (see discussion surrounding Figure 3 in section 3.1). Table 4 indicates that CT

dx.doi.org/10.1021/jp501815j | J. Phys. Chem. B 2014, 118, 8330−8351

component of $\Delta\langle\mu\rangle_{10}$ is significant for all three of Figure 1's complexes, a feature consistent with some current H-bonding theories.[38,45,46] For the phenol−DSMO complex, the proton stretch component contributes 55−60% to the slope, while the CT component contributes 45−40%, with the latter increasing with increased solvent polarity. Even for the weaker ethanol−DMSO complex, where CT is expected to be the least due to the larger ΔPA and H-bond length, the $\Delta\langle\mu\rangle_{10}$ CT contribution to the slope is significant, ∼20%.

5.3.2. Nonpolar Solvent Slope. We now turn to the nonpolar solvent slopes. It is useful to use eq 42 and divide the slope eq 44, into non-CT (1st term) and CT components (2nd term)

$$\frac{\mathrm{d}h\nu}{\mathrm{d}(1/\varepsilon)} = M_S\{\langle\mu_N^2(q,Q)\rangle_{eq1} - \langle\mu_N^2(q,Q)\rangle_{eq0}\} + M_S[\langle c_I^2(q,Q)\{\mu_I^2(q,Q) - \mu_N^2(q,Q)\}\rangle_{eq1} - \langle c_I^2(q,Q)\{\mu_I^2(q,Q) - \mu_N^2(q,Q)\}\rangle_{eq0}] \quad (58)$$

Each term involves averages over various first- and second-order nuclear terms because squared (q,Q)-dependent diabatic dipole moments occur (see eqs 45−47).

Table 5 presents the values of the nonpolar slope and its non-CT and CT components (eq 58), as well as a numerical verification of the validity of eq 58. Just as was the case for the polar solvent slope results in section 5.3, the nonpolar solvent slope's CT contribution increases with the acid's acidity (i.e., with decreasing ΔPA, eq 50). The CT contribution makes up >40% of the slope; this is larger than for the polar slope case, due to the purely equilibrium solvation nature of nonpolar solvation, resulting in increased ionic state population c_I^2.

Finally, we comment on the linearity of the proton frequency curves for solvents in Figure 1. The nonpolar solvent version of the polar solvent eq 55 is an integral over the nonpolar expression eq 58

$$h\nu_{NP}(\varepsilon,\varepsilon_\infty) = h\nu_{AH}(\varepsilon=\varepsilon_\infty=2) - \int_{1/2}^{1/\varepsilon_\infty}\left(\frac{\mathrm{d}h\nu_{AH}(\varepsilon,\varepsilon_\infty)}{\mathrm{d}(1/\varepsilon)}\right)_{NP}\mathrm{d}(1/\varepsilon_\infty) \approx h\nu_{AH}(\varepsilon=\varepsilon_\infty=2) + \left.\frac{\mathrm{d}h\nu_{AH}(\varepsilon)}{\mathrm{d}(1/\varepsilon)}\right|_{\varepsilon=\varepsilon_\infty}\left(\frac{1}{2}-\frac{1}{\varepsilon_\infty}\right) \quad (59)$$

with integration limits from $\varepsilon=\varepsilon_\infty=2$ for the reference solvent to the specific ε_∞ value $\varepsilon=\varepsilon_\infty$. Approximating the nonpolar slope as constant generates the second, linear expression.[137] We forego a nonpolar solvent figure analogous to Figure 9b for polar solvents to address any nonlinearity of the nonpolar behavior; instead, we simply state that all nonpolar solvent slopes in Figure 1 vary by less than 10%, which is on the order of the error of a linear fit of the experimental data. This fairly linear behavior stems primarily from the limited ε_∞ variation for these solvents.

6. CONCLUDING REMARKS

In this contribution, we have presented a theory for the proton stretch vibrational frequency ν_{AH} in an H-bonded complex and its variation with $1/\varepsilon$, the inverse of the solvent dielectric constant and successfully compared its predictions with recent experimental results.[18] Important aspects of the theory include focus on a H-bonded complex itself dissolved in a solvent (thus paying attention to specific acid−base H-bond interactions), a two VB state approach to the electronic structure, quantization of the proton and H-bond coordinates of the complex, and attention to nonequilibrium solvation issues for both the solvation and the Franck−Condon vibrational transitions. As noted in the Introduction, many of these aspects, which are quite important for the frequency and its solvent dependence, are absent in prior theoretical approaches. The evaluation of the theoretical expressions for the proton frequencies and their variations with solvent involves some electronic structure calculations, some vacuum molecular parameters, and some parametrization. The latter is done for a reference nonpolar solvent and is then employed for other nonpolar solvents and for polar solvents.

According to the theory, the ν_{AH} magnitude depends on solvation factors for the H-bonded complex, namely its size and dipole moment, and on the difference in acidity between the acid proton donor and the base proton acceptor, measured by an appropriate difference in proton affinities. This acidity is also strongly related to charge transfer (CT) in the vibrational transition whose description is allowed by the VB approach. The acidity is the dominant factor for the ν_{AH} magnitude, while it and the solvation factors clearly determine the variation with ε. The experimental and theoretical ν_{AH} variation with $1/\varepsilon$ displayed in Figure 1 depends on whether the solvents are polar or nonpolar and is quantitatively described via the theoretical slope expressions in eqs 39 and 44, respectively. The approximate linearity seen in Figure 1 is primarily due to a ground vibrational state H-bonded complex dipole moment that varies little with ε, as well as a structure factor M_S that is ε-independent. These slopes are characteristically dependent on the H-bonded complex size, dipole moment, and acidity/CT.

We especially wish to emphasize the overall importance of acidity and CT, which are themselves coupled to the proton potential anharmonicity, all of which are reflected in the ionic VB state's electronic contribution. The impacts of CT and acidity are significant for the frequency and its solvent dependence. Our predicted red-shift increase with a larger CT contribution is consistent with H-bond trends for acidity, H-bond strength, and CT.[1−8,38,44,45] The acidity effects for the both the ν_{AH} magnitude and ε-dependence will become even more evident in the application of this theory to H-bonded complexes, which are similar in structure but which differ primarily in acidity.

Experimental analysis of PT in the excited electronic state via photoacids[139−141] and photobases[142−145] has played an important role in understanding acidity and H-bonding. Application/extension of the present theoretical approach to IR absorption in the excited electronic state is of obvious interest and is underway. One significant difference from the ground electronic state situation discussed here is the likely involvement of more than two VB states, one of which must account for the source of the greatly enhanced acidity arising from a different CT in the excited electronic S1 state.[146,147]

APPENDIX A

Free Energy Derivatives

In this Appendix, expressions for the free energy $G(q,Q,s)$ derivatives with respect to both the solvent coordinate s and $\mathcal{R}$ are presented. These allow for the derivation of the equilibrium solvent coordinate s_{eq0} expression (eq 30) and the $G(q,Q,s)$

dx.doi.org/10.1021/jp501815j | J. Phys. Chem. B 2014, 118, 8330−8351

derivative with respect to K (eq 34). We begin the free energy, which, from eqs 19 and 20, is

$$G(q, Q, s) = \frac{V_N^{\infty}(q, Q) + V_I^{\infty}(q, Q)}{2} - \frac{(\mu_I(q, Q) + \mu_N(q, Q))\mathcal{R}(s)}{2} + \frac{1}{2K}\mathcal{R}(s)^2 - \frac{1}{2}\left[\{V_I^{\infty}(q, Q) - V_N^{\infty}(q, Q) - (\mu_I(q, Q) - \mu_N(q, Q))\mathcal{R}(s)\}^2 + 4\beta(Q)^2\right]^{1/2} \quad (A.1)$$

where the only s dependence is contained in $\mathcal{R}(s)$. The equilibrium s position in the ground vibrational state $\mathcal{E}_0$ requires the derivative $dG(q,Q,s)/ds$ (see eq 29), which is decomposed as

$$\frac{dG(q, Q, s)}{ds} = \frac{\partial G(q, Q, s)}{\partial \mathcal{R}(s)}\frac{d\mathcal{R}(s)}{ds} \quad (A.2)$$

Because the second derivative in eq A.2 is s-independent (see eq 16),

$$\frac{d\mathcal{R}(s)}{ds} = K(\tilde{\mu}_I - \tilde{\mu}_N) \quad (A.3)$$

the eq 28 equilibrium condition is now transformed into an equilibrium condition for the reaction field $\mathcal{R}(s)$

$$\langle \phi_0(q, Q, s) \left| \frac{\partial G(q, Q, s)}{\partial \mathcal{R}(s)} \right| \phi_0(q, Q, s) \rangle = 0 \quad (A.4)$$

From eq A.1 and eq 21 relation, the partial derivative here is

$$\frac{\partial G(q, Q, s)}{\partial \mathcal{R}(s)} = \left[-\frac{(\mu_I(q, Q) + \mu_N(q, Q))}{2} + \frac{\mathcal{R}(s)}{K} - \left(c_I^2(q, Q, s) - \frac{1}{2}\right)(\mu_I(q, Q) - \mu_N(q, Q)) \right] = \left[\frac{\mathcal{R}(s)}{K} - \mu(q, Q, s) \right] \quad (A.5)$$

where eq 5 relation dipole μ relation was used to obtain the second line. Inserting this into eq A.4 gives the expected relationship between the equilibrium reaction field and the equilibrium dipole moment

$$\mathcal{R}_{eq0} = K\langle \mu \rangle_{eq0} \quad (A.6)$$

This result, together with the $\mathcal{R}$ definition eq 16, yields from eq A.5 the desired result (eq 36).

APPENDIX B

Valence Bond Potentials

The form and parametrization of the VB potentials $V_{N,I}$ from eq 44 are presented in this Appendix. We begin with the vacuum AH and HB proton stretch potentials V_{AH} and V_{HB+}, described by Morse potentials

$$V_{AH}(q) = D_{AH}[1 - \exp\{-a_{AH}(q - r_{AH})\}]^2; \quad V_{HB+}(Q - q) = D_{BH}[1 - \exp\{-a_{BH}(Q - q - r_{BH})\}]^2 \quad (B.1)$$

The V_{AH} and V_{HB+} parameters for eq B.1 (see Table 6) are taken to be consistent with an AH (HB^+) bond dissociation energy[110] and gas phase stretch vibrational frequency.

The neutral state V_{nHB} net non-bonding interaction is modeled by a Morse potential and a repulsive term:

$$V_{nHB}(Q - q) = D_{nOH}[1 - \exp\{-a_{nOH}(Q - q - r_{nOH})\}]^2 + \varepsilon_{rep}[\sigma_{rep}/(Q - q)]^{12} \quad (B.2)$$

For the ionic state, an extra electrostatic interaction is added to account for the interaction between the proton and the donor, which has a net $-1e$ charge

$$V_{nAH}(q) = -\frac{0.5}{4}\frac{e^2}{q} + D_{nOH}[1 - \exp\{-a_{nOH}(q - r_{nOH})\}]^2 + \varepsilon_{rep}[\sigma_{rep}/q]^{12} \quad (B.3)$$

Equations B.2 and B.3 were constructed such that only the Morse parameters need modification during the final parametrization. The electrostatic term in eq B.3 is one-quarter that of the expected interaction between $0.5e$ and $-1e$ charges because a significant portion of that attractive interaction is contained within the Morse term. The diminished electrostatic component ensures that V_I has a single proton potential minimum localizing the proton with the acceptor B. A full electrostatic interaction $-0.5e^2/q$ would produce a double well proton potential, where the proton could also be localized near the acid A in the ionic diabatic state, inconsistent with the character of the complexes assumed for our treatment.

The 12th order repulsive terms in eqs B.2 and B.3 (ε_{rep} = 0.4 kcal/mol; σ_{rep} = 1 Å) ensure proper boundary conditions for the proton at A and B. Specifically, this term enables the difference $V_N - V_I$ to always be large and positive for q near 0 and large and negative for q near the base. This behavior ensures that c_I^2 in eq 21 appropriately approaches 0 and 1, respectively.

For the H-bond interaction, the nonbonded interactions V_{nHB} and V_{nAH} also appropriately contribute to the H-bond mode, via an attraction between the proton and the nonbonded proton donor/acceptor, indicated by the electrostatic term in eq B.3 and the Q dependence in eq B.2. The last component in eq 44 $V_{N,I,AB}$ is the other contribution to the A···B interaction, which is taken for the neutral state as a Morse potential

$$V_{N,AB}(Q) = D_{OO}[1 - \exp\{-a_{OO}(Q - r_{OO})\}]^2 \quad (B.4)$$

The ionic state includes an extra electrostatic term with a coefficient C_{Qelec} corresponding to the attraction between the oppositely charged A and B moieties

$$V_{I,AB} = D_{OO}[1 - \exp\{-a_{OO}(Q - r_{OO})\}]^2 - \frac{C_{Qelec}e^2}{Q} + 4\varepsilon_{OO}\left[\left(\frac{\sigma_{OO}}{Q}\right)^{12} - \left(\frac{\sigma_{OO}}{Q}\right)^{6}\right] \quad (B.5)$$

The Lennard-Jones potential in eq B.5 is part of the ionic nonbonding interaction between the charged oxygens, with parameters consistent with an O−O interaction[125] (ε_{OO} = 0.18 kcal/mol; σ_{OO} =3.24 Å). The value used for C_{Qelec} is determined from an estimation of the equilibrium vacuum gap between the minima in q of the two VB states for $Q = Q_{eq}$,

dx.doi.org/10.1021/jp501815j | J. Phys. Chem. B 2014, 118, 8330−8351

which is essentially the difference in H-bond energy between the neutral and ionic state evaluated at Q_{eq}, defined from

$$\langle V_N(q_{N,min}, Q)\rangle_{eq0} - \langle V_I(q_{I,min}, Q)\rangle_{eq0} = \Delta_Q - \Delta PA \tag{B.6}$$

From the above definitions of the diabatic potentials V_N and V_I, Δ_Q is the sum of the extra electrostatic contributions for the ionic state

$$\begin{aligned}\Delta_Q &\approx -4\varepsilon_{OO}\left[\left(\frac{\sigma_{OO}}{Q_{eq}}\right)^{12} - \left(\frac{\sigma_{OO}}{Q_{eq}}\right)^{6}\right] - \left[-\frac{C_{Qelec}e^2}{Q_{eq}} - \frac{1}{8}\frac{e^2}{q_{I,min}}\right] \\ &= -4\varepsilon_{OO}\left[\left(\frac{\sigma_{OO}}{Q_{eq}}\right)^{12} - \left(\frac{\sigma_{OO}}{Q_{eq}}\right)^{6}\right] \\ &\quad - \left[-\frac{C_{Qelec}e^2}{Q_{eq}} - \frac{1}{8}\frac{e^2}{(Q_{eq} - q_o)}\right]\end{aligned} \tag{B.7}$$

The only variable eq B.7 parameter is the electrostatic interaction prefactor, C_{Qelec}, of the donor and acceptor atoms in the ionic state.

From a vacuum quantum chemistry calculation of the $Q = Q_{eq\infty}$ equilibrium complex, the vacuum offset is estimated by the difference in potential energy from the proton potential minimum q ~1 Å and the inflection point on the proton potential indicating the minimum of the ionic VB potential (i.e., $q \sim Q-1$ Å). The basis set and level of theory for these vacuum calculations are MP2/6-311++G**.[93] Obviously, this estimate is a lower limit, but the endergonicity is great enough such that this estimate is likely only a few percent of the expected. Further note that we are NOT trying to exactly reproduce the $Q = Q_{eq}$ vacuum proton potential because the ν_{OH} of that proton potential or even the corresponding $\varepsilon_\infty = 2$ solvent proton potential does not equate with the corresponding experimental ν_{OH} value. The eqs B.4 and B.5 Morse parameters and C_{Qelec} are listed in Table 7 and are consistent with the equilibrium H-bond separation in the ε_∞ solvent, whose geometry can be found in section 4.1.

■ ASSOCIATED CONTENT

Supporting Information

Detailed discussion of the H-bond characteristics that determine M_S magnitude and its ε (in)dependence. This material is available free of charge via the Internet at http://pubs.acs.org.

■ AUTHOR INFORMATION

Corresponding Authors

*E-mail: Philip.Kiefer@colorado.edu.
*E-mail: James.Hynes@colorado.edu.

Notes

The authors declare no competing financial interest.

■ ACKNOWLEDGMENTS

This work was supported in part by United States−Israel Binational Science Foundation Grant No. 2006276 (E.P., J.T.H.) and by NSF Grant No. CHE-1112564 (J.T.H.).

■ REFERENCES

(1) Bell, R. P. *The Proton in Chemistry*, 2nd ed.; Cornell University Press: Ithaca, NY, 1973.
(2) Caldin, E.; Gold, V. *Proton Transfer Reactions*; Chapman and Hall: London, 1975.
(3) Hynes, J. T., Klinman, J. P., Limbach, H. H., Schowen, R. L., Eds. *Hydrogen-Transfer Reactions*; Wiley-VCH Verlag GmbH & Co. KGaA: Weinheim, Germany, 2007.
(4) Elsaesser, T., Bakker, H. J., Eds. *Ultrafast Hydrogen Bonding Dynamics and Proton Transfer Processes in the Condensed Phase*; Kluwer Academic Publishers: Amsterdam, 2002.
(5) Hibbert, F. Mechanisms of Proton Transfer between Oxygen and Nitrogen Acids and Bases in Aqueous Solution. *Adv. Phys. Org. Chem.* **1986**, *22*, 113−212.
(6) Hibbert, F.; Emsley, J. Hydrogen Bonding and Chemical Reactivity. *Adv. Phys. Org. Chem.* **1990**, *26*, 255−379.
(7) (a) Pimentel, G. C. *The Hydrogen Bond*; W. H. Freeman: San Francisco, 1960. (b) Novak, A. Hydrogen Bonding in Solids: Correlation of Spectroscopic and Crystallographic Data. *Struct. Bonding (Berlin, Ger.)* **1974**, *18*, 177−216.
(8) Joesten, M. D.; Schaad, L. J. *Hydrogen Bonding*; Marcel Dekker, Inc.: New York, 1974.
(9) Fersht, A. *Structure and Mechanism in Protein Science: A Guide to Enzyme Catalysis and Protein Folding*; W.H. Freeman: New York, 1999.
(10) Cleland, W. W.; Kreevoy, M. M. Low-Barrier Hydrogen Bonds and Enzymic Catalysis. *Science* **1994**, *264*, 1887−1890.
(11) Cleland, W. W.; Frey, P. A.; Gerlt, J. A. The Low Barrier Hydrogen Bond in Enzymatic Catalysis. *J. Biol. Chem.* **1998**, *273*, 25529−25532.
(12) Kamlet, M. J.; Solomonovici, A.; Taft, R. W. Linear Solvation Energy Relationships. 5. Correlations between Infrared $\Delta\nu$ Values and the π Scale of Hydrogen Bond Acceptor Basicities. *J. Am. Chem. Soc.* **1979**, *101*, 3734−3739.
(13) Kamlet, M. J.; Gal, J.-F.; Maria, P.-C.; Taft, R. W. Linear solvation energy relationships. Part 32. A co-ordinate covalency parameter, ξ, which, in combination with the hydrogen bond acceptor basicity parameter, β, permits correlation of many properties of neutral oxygen and nitrogen bases (including aqueous pK_a). *J. Chem. Soc., Perkin Trans. 2* **1985**, 1583−1589.
(14) Kamlet, M. J.; Abboud, J. L.; Taft, R. W. The Solvatochromic Comparison Method. 6. The π^* Scale of Solvent Polarities. *J. Am. Chem. Soc.* **1977**, *99*, 6027−6038.
(15) Taft, R. W.; Abboud, J. L.; Kamlet, M. J. Linear Solvation Energy Relationships. 23. A Comprehensive Collection of the Solvatochromic Paramaters, π^*, α, and β, and Some Methods for Simplifying the Generalized Solvatochromic Equation. *J. Org. Chem.* **1984**, *49*, 2001−2005.
(16) Taft, R. W.; Abboud, J. L.; Kamlet, M. J. Solvatochromic Comparison Method. 20. Linear Solvation Energy Relationships. 12. The δ Term in the Solvatochromic Equations. *J. Am. Chem. Soc.* **1981**, *103*, 1080−1086.
(17) Kirkwood, J. G. Theory of Solutions of Molecules Containing Widely Separated Charges with Special Application to Zwitterions. *J. Chem. Phys.* **1934**, *2*, 351−361.
(18) Keinan, S.; Pines, D.; Kiefer, P. M.; Hynes, J. T.; Pines, E. Solvent Induced O-H Vibration Red-Shifts in Hydrogen-Bonded Acid−Base Complexes. *J. Chem. Phys. B*, submitted for publication, **2014**.
(19) Bauer, P. E.; Magat, M. Sur la Déformation des Molécules en Phase Condensée et la liaison hydrogen. *J. Phys. Radium* **1938**, *9*, 319−330.
(20) Onsager, L. Electric Moments of Molecules in Liquids. *J. Am. Chem. Soc.* **1936**, *58*, 1486−1493.
(21) Böttcher, C. J. F. *Theory of Electric Polarization*; Elsevier: Amsterdam, 1952.
(22) Buckingham, A. D. Solvent Effects in Infrared Spectroscopy. *Proc. R. Soc. London, Ser. A* **1958**, *248*, 169−182.
(23) Pullin, A. D. E. The Variation of Infrared Vibration Frequencies with Solvent. *Spectrochim. Acta* **1958**, *13*, 125−138.

(24) Pullin, A. D. E. Solution Frequency Shift and Solvent Refractive Index. *Spectrochim. Acta* **1960**, *16*, 12−24.
(25) Rao, C. N. R.; Singh, S.; Senthilnathan, V. P. Spectroscopic Studies of Solute-Solvent Interactions. *Chem. Soc. Rev.* **1976**, *5*, 297−316.
(26) Wong, M. H.; Wiberg, K. B.; Frisch, M. Hartree−Fock Second Derivatives and Electric Field Properties in a Solvent Reaction Field: Theory and Application. *J. Chem. Phys.* **1991**, *95*, 8991−8998.
(27) Cappelli, C.; Mennucci, B.; da Silva, C. O.; Tomasi, J. Refinements on Solvation Continuum Models: Hydrogen-Bond Effects on the OH Stretch in Liquid Water and Methanol. *J. Chem. Phys.* **2000**, *112*, 5382−5392.
(28) Cammi, R.; Cappelli, C.; Corni, S.; Tomasi, J. On the Calculation of Infrared Intensities in Solution within the Polarizable Continuum Model. *J. Phys. Chem. A* **2000**, *104*, 9874−9879.
(29) Cappelli, C.; Corni, S.; Cammi, R.; Mennucci, B.; Tomasi, J. Nonequilibrium formulation of infrared frequencies and intensities in solution: Analytical evaluation within the polarizable continuum model. *J. Chem. Phys.* **2000**, *113*, 11270−11279.
(30) van der Zwan, G.; Hynes, J. T. Time-Dependent Fluorescence Solvent Shifts, Dielectric Friction, and Nonequilibrium Solvation in Polar Solvents. *J. Phys. Chem.* **1985**, *89*, 4181−4188.
(31) Asbury, J. B.; Wang, Y.; Lian, T. Time-Dependent Vibration Stokes Shift during Solvation: Experiment and Theory. *Bull. Chem. Soc. Jpn.* **2002**, *75*, 973−983.
(32) Prémont-Schwarz, M.; Xiao, D.; Batista, V.; Nibbering, E. T. J. The O−H Stretching Mode of a Prototypical Photoacid as a Local Dielectric Probe. *J. Phys. Chem. A* **2011**, *115*, 10511−10516.
(33) Xiao, D.; Prémont-Schwarz, M.; Batista, V.; Nibbering, E. T. J. Ultrafast Vibrational Frequency Shifts Induced by Electronic Excitations: Naphthols in Low Dielectric Media. *J. Phys. Chem. A* **2011**, *116*, 2775−2790.
(34) Timoneda, J. J.; Hynes, J. T. Nonequilibrium Free Energy Surfaces for Hydrogen-Bonded Proton Transfer Complexes in Solution. *J. Phys. Chem.* **1991**, *95*, 10431−10442.
(35) Kiefer, P. M.; Hynes, J. T. Theoretical Aspects of Proton Transfer Reactions in a Polar Environment. In *Hydrogen-Transfer Reactions*; Hynes, J. T., Klinman, J. P., Limbach, H. H., Schowen, R. L., Eds.; Wiley-VCH Verlag GmbH & Co. KGaA: Weinheim, Germany, 2007, Vol. *1*, pp 303−348.
(36) Kiefer, P. M.; Hynes, J. T. Nonlinear Free Energy Relations for Adiabatic Proton Transfer Reactions in a Polar Environment. I. Fixed Proton Donor-Acceptor Distance. *J. Phys. Chem. A* **2002**, *106*, 1834−1849.
(37) Kiefer, P. M.; Hynes, J. T. Nonlinear Free Energy Relations for Adiabatic Proton Transfer Reactions in a Polar Environment. II. Inclusion of Proton Donor-Acceptor Vibration. *J. Phys. Chem. A* **2002**, *106*, 1850−1861.
(38) Thompson, W. H.; Hynes, J. T. Frequency Shifts in the Hydrogen-Bonded OH Stretch in Water-Halide Clusters. The Importance of Charge Transfer. *J. Am. Chem. Soc.* **2000**, *122*, 6278−6286.
(39) Thompson, W. H.; Hynes, J. T. A Model Study of the Acid-Base Proton Transfer Reaction of the $ClH\cdots OH_2$ Pair in Low Polarity Solvents. *J. Phys. Chem. A* **2001**, *105*, 2582−2590.
(40) Kiefer, P. M.; Hynes, J. T. Temperature-Dependent Solvent Polarity Effects on Adiabatic Proton Transfer Rate Constants and Kinetic Isotope Effects. *Isr. J. Chem.* **2004**, *44*, 171−184.
(41) Allerhand, A.; von Schleyer, P. R. Solvent Effects in Infrared Spectroscopic Studies of Hydrogen Bonding. *J. Am. Chem. Soc.* **1963**, *85*, 371−380.
(42) McDowell, S. A. C.; Buckingham, A. D. On the Correlation between Bond-Length Change and Vibrational Frequency Shift in Hydrogen-Bonded Complexes: A Computational Study of Y···HCl Dimers (Y = N2, CO, BF). *J. Am. Chem. Soc.* **2005**, *127*, 15515−15520.
(43) The importance of charge transfer for the proton stretch frequencies of gas phase H-bond clusters using a two VB model was emphasized in ref 38. See also Robertson, W. H.; Johnson, M. A. Molecular Aspects Of Halide Ion Hydration: The Cluster Approach. *Annu. Rev. Phys. Chem.* **2003**, *54*, 173−213 For reviews on the charge transfer contribution to H-bond energies, see refs 44−46.
(44) Morokuma, K. Why do molecules interact? The origin of electron donor-acceptor complexes, hydrogen bonding, and proton affinity. *Acc. Chem. Res.* **1977**, *10*, 294−300.
(45) Reed, A. E.; Curtiss, L. A.; Weinhold, F. Intermolecular interactions from a natural bond orbital, donor-acceptor viewpoint. *Chem. Rev.* **1988**, *88*, 899−926.
(46) Ramos-Cordoba, E.; Lambrecht, D. S.; Head-Gordon, M. Charge-transfer and the hydrogen bond: Spectroscopic and structural implications from electronic structure calculations. *Faraday Discuss.* **2011**, *150*, 345−362.
(47) A more realistic description of vibrational dynamics goes beyond the static picture to include structural flexibility that H-bonds exhibit. For a description of such techniques with fluxionality, see refs 46 and 48.
(48) McCoy, A. B. Diffusion Monte Carlo Approaches for Investigating the Structure and Vibrational Spectra of Fluxional Systems. *Int. Rev. Phys. Chem.* **2006**, *25*, 77−107.
(49) Skinner, J.; Auer, B. M.; Lin, Y.-S. Vibrational Line Shapes, Spectral Diffusion, and Hydrogen Bonding in Liquid Water. *Adv. Chem. Phys.* **2009**, *142*, 59−103.
(50) Bakker, H. J.; Skinner, J. L. Vibrational Spectroscopy as a Probe of Structure and Dynamics in Liquid Water. *Chem. Rev.* **2010**, *110*, 1498−1517.
(51) Riddick, J. A.; Bunger, W. B.; Sakano, T. K. *Organic Solvents. Physical Properties and Methods of Purification*, 4th ed.; Techniques of Chemistry; John Wiley & Sons: New York, 1986.
(52) Reichardt, C. *Solvents and Solvent Effects in Organic Chemistry*; Wiley-VCH: Weinheim, Germany, 1988.
(53) Kim, H. J.; Hynes, J. T. Equilibrium and Nonequilibrium Solvation and Solute Electronic Structure. I. Formulation. *J. Chem. Phys.* **1990**, *93*, 5194−5210.
(54) Kim, H. J.; Hynes, J. T. Equilibrium and Nonequilibrium Solvation and Solute Electronic Structure. II. Strong Coupling Limit. *J. Chem. Phys.* **1990**, *93*, 5211−5223.
(55) Kim, H. J.; Hynes, J. T. Equilibrium and Nonequilibrium Solvation and Solute Electronic Structure. III. Quantum Theory. *J. Chem. Phys.* **1992**, *96*, 5088−5110.
(56) Lee, S.; Hynes, J. T. Solution Phase Reaction Path Hamiltonian. I. Formulation. *J. Chem. Phys.* **1988**, *88*, 6853−6862.
(57) Lee, S.; Hynes, J. T. Solution Phase Reaction Path Hamiltonian. II. Applications. *J. Chem. Phys.* **1988**, *88*, 6863−6870.
(58) Bergsma, J. P.; Gertner, B. J.; Wilson, K. R.; Hynes, J. T. Molecular Dynamics of a Model S_N2 Reaction in Water. *J. Chem. Phys.* **1987**, *86*, 1356−1376.
(59) Gertner, B. J.; Bergsma, J. P.; Wilson, K. R.; S. Lee, S.; Hynes, J. T. Nonadiabatic Solvation Model for S_N2 Reactions in Polar Solvents. *J. Chem. Phys.* **1987**, *86*, 1377−1386.
(60) Mathis, J. R.; Kim, H. J.; Hynes, J. T. A Theoretical Model for S_N1 Ionic Dissociations in Solution. III. Analysis of t-Butyl Halide. *J. Am. Chem. Soc.* **1993**, *115*, 8248−8262.
(61) An extensive list of theoretical and computational studies using a large electronic coupling (∼1 eV) for H-bond systems is given in Kiefer, P. M.; Hynes, J. T. Theoretical Aspects of Tunneling Proton Transfer Reactions in a Polar Environment. *J. Phys. Org. Chem.* **2010**, *23*, 632−646.
(62) Kiefer, P. M.; Hynes, J. T. Kinetic Isotope Effects for Adiabatic Proton Transfer Reactions in a Polar Environment. *J. Phys. Chem. A* **2003**, *107*, 9022−9039.
(63) In reality, the $\boldsymbol{\mu}$, $\boldsymbol{\mu}_N$, and $\boldsymbol{\mu}_I$ vectors need not point in the same direction. While a 2D version of the theory could be implemented that includes dipole moment components parallel and perpendicular to the H-bond axis, we ignore this complication for the simple evaluation of the theory for the systems considered here. Further, quantum chemistry calculations varying the proton position between the donor and acceptor atoms in the equilibrium structures obtained in

section 4.1 indicate that the dipole moments in the neutral and ionic states are fairly collinear.
(64) Because the neutral and ionic states are appropriately defined with Löwdin orthogonalized diabatic states (cf. ref 34), the resulting $\mu_{N,I}$ is effectively zero.
(65) This assumption cannot be invoked for H-bond solvents such as water, where, for example, rapid OH librations, which should be important for electric field (and potential) fluctuations experienced by the complex, are simply not fast compared to the H-bond coordinate of the complex.
(66) The following ref and refs 67−69 are examples of the equilibrium solvation picture for PT in a complex system: Bash, P. A.; Field, M. J.; Davenport, R. C.; Petsko, G. A.; Ringe, D.; Karplus, M. Computer Simulation and Analysis of the Reaction Pathway of Triosephosphate Isomerase. *Biochemistry* **1991**, *30*, 5826−5832.
(67) Cui, Q.; Karplus, M. Triosephosphate Isomerase: A Theoretical Comparison of Alternative Pathways. *J. Am. Chem. Soc.* **2001**, *123*, 2284−2290.
(68) Alhambra, C.; Corchado, J.; Sánchez, M. L.; Garcia-Viloca, M.; Gao, J.; Truhlar, D. G. Canonical Variational Theory for Enzyme Kinetics with the Protein Mean Force and Multidimensional Quantum Mechanical Tunneling Dynamics. Theory and Application to Liver Alcohol Dehydrogenase. *J. Phys. Chem. B* **2001**, *105*, 11326−11340.
(69) Cui, Q.; Elstner, M.; Karplus, M. A Theoretical Analysis of the Proton and Hydride Transfer in Liver Alcohol Dehydrogenase (LADH). *J. Phys. Chem. B* **2002**, *106*, 2721−2740.
(70) Marcus, R. A. Electrostatic Free Energy and Other Properties of States Having Nonequilibrium Polarization. I. *J. Chem. Phys.* **1956**, *24*, 979−989.
(71) Marcus, R. A. Free Energy of Nonequilibrium Polarization Systems. II. Homogeneous and Electrode Systems. *J. Chem. Phys.* **1963**, *38*, 1858−1862.
(72) Marcus, R. A. Free Energy of Nonequilibrium Polarization Systems. III. Statistical Mechanics of Homogeneous and Electrode Systems. *J. Chem. Phys.* **1963**, *39*, 1734−1740.
(73) This also accounts for the different dielectric factors in the present work compared to those in point dipole treatments of a solute.[20−25,30−33]
(74) Kiefer, P. M.; Hynes, J. T. Kinetic Isotope Effects for Nonadiabatic Proton Transfer Reactions in a Polar Environment I. Interpretation of Tunneling Kinetic Isotope Effects. *J. Phys. Chem. A* **2004**, *108*, 11793−11808.
(75) Kiefer, P. M.; Hynes, J. T. Kinetic Isotope Effects for Nonadiabatic Proton Transfer Reactions in a Polar Environment II. Comparison with an Electronically Diabatic Perspective. *J. Phys. Chem. A* **2004**, *108*, 11809−11818.
(76) In the free energy differences between G_n levels, as well as those with G_n and G_{min}, entropic solvation effects cancel out, leaving only nuclear vibrational energy level separations. For example, G_0-G_{min} yields the zero point energy.[35−37,62,77,78]
(77) Ando, K.; Hynes, J. T. HF Acid Ionization in Water: The First Step. *Faraday Soc. Discuss.* **1995**, *102*, 435−441.
(78) Ando, K.; Hynes, J. T. Molecular Mechanism of HCl Acid Ionization in Water. Ab Initio Potential Energy Surfaces and Monte Carlo Simulations. *J. Phys. Chem. B* **1997**, *101*, 10464−10478.
(79) Gertner, B. J.; Hynes, J. T. Model Molecular Dynamics Simulation of Hydrochloric Acid Ionization at the Surface of Stratospheric Ice. *Faraday Soc. Discuss.* **1998**, *110*, 301−322.
(80) The equilibrium solvent coordinate value s_{eq1} in the vibrationally excited state differs from the ground state value s_{eq0}, a feature related to a vibrational Stokes shift. Within the present model, this shift is the difference in the eq 27 energy gap for $s = s_{eq0}$ and $s = s_{eq1}$: $h\nu(s_{eq0}) - h\nu(s_{eq1}) = G_1(s_{eq0}) - G_0(s_{eq0}) - G_1(s_{eq1}) + G_0(s_{eq1})$. This shift will increase with increasing the force constant K, which is larger for smaller H-bonded complexes when $\varepsilon \gg \varepsilon_\infty$ (eq 14). For the present complexes, the Stokes shifts are quite small (< 5 cm^{-1}) because these complexes are relatively large. More important shifts are observed for HOD in D_2O.[81,82]
(81) Woutersen, S.; Bakker, H. J. Hydrogen Bond in Liquid Water as a Brownian Oscillator. *Phys. Rev. Lett.* **1999**, *83*, 2077−2080.
(82) Wang, Z.; Pang, Y.; Dlott, D. D. The Vibrational Stokes Shift of Water (HOD in D_2O). *J. Chem. Phys.* **2004**, *120*, 8345−8348.
(83) For a discussion of the Hellman−Feynman theorem, see chapter 14 in Levine, I. N. *Quantum Chemistry*, 4th ed., Prentice Hall: Upper Saddle River, NJ, 1991.
(84) Sheppard, N. Infrared Spectroscopy and Hydrogen Bonding—Band Widths and Frequency and Frequency Shifts. In *Hydrogen Bonding*, Hadzi, D., Ed.; Pergamon Press, Ltd.: London, 1959; pp 85−106.
(85) Staib, A.; Hynes, J. T. Vibrational Predissociation in Hydrogen-Bonded OH···O Complexes via OH Stretch—OO Stretch Energy Transfer. *Chem. Phys. Lett.* **1993**, *204*, 197−203.
(86) Klippenstein, S. K.; Hynes, J. T. Direct and Indirect Solvent Coupling Mechanisms for Vibrational Dephasing in Hydrogen-Bonded Molecules. *J. Phys. Chem.* **1991**, *95*, 4651−4659.
(87) The basic form of eq 38 or 39 is reminiscent of the first order vibrational Stark (cf. Hush, N. S.; Reimers, J. R. Vibrational Stark Spectroscopy. 1. Basic Theory and Application to the CO Stretch. *J. Phys. Chem.* **1995**, *99*, 15798−15805 and refs 88 and 89), where the absorption energy change is the difference in the dipole moment for the two states times the change in external field. This is made more explicit in the differential form $d h\nu = -(\langle\mu\rangle_{eq1} - \langle\mu\rangle_{eq0})\, d\mathcal{R}_{eq0}$, relating the frequency change to the change in the solvent's equilibrium orientational polarization reaction field in the ground vibrational state (see the discussion above eq 11 for the sense of "equilibrium" here). While this connection provides some physical perspective for eqs 38 and 39, there are strong differences. Specifically, the orientational polarization's reaction field is not an independent external field, and there is an additional frequency-shifting solvent electronic polarization field effect on the ground and excited vibrational state wavefunctions.
(88) Hochstrasser, R. M. Electric Field Effects on Orientated Molecules and Molecular Crystals. *Acc. Chem. Res.* **1973**, *6*, 263−269.
(89) Bublitz, G. U.; Boxer, S. G. Stark Spectroscopy: Applications in Chemistry, Biology, and Materials Science. *Annu. Rev. Phys. Chem.* **1997**, *48*, 213−242.
(90) Eqs 38 and 39 should apply in general to molecular vibrations of polar molecules in a polar solvent. Further, their simple structure also suggests that similar equations could apply for more refined descriptions of the complex's charge distribution (e.g., point charges); in that case, reaction potentials would appear rather than reaction fields. Similar statements apply to the nonpolar solvent eq 43.
(91) Becke, A. D. Density-Functional Thermochemistry. III. The Role of Exact Exchange. *J. Chem. Phys.* **1993**, *98*, 5648−5652.
(92) Lee, C.; Yang, W.; Parr, R. G. Development of the Colle−Salvetti correlation-energy formula into a functional of the electron density. *Phys. Rev. B* **1988**, *37*, 785−789.
(93) Krishnan, R.; Binkley, J. S.; Seeger, R.; Pople, J. A. Self-Consistent Molecular Orbital Methods. XX. A Basis Set for Correlated Wave Functions. *J. Chem. Phys.* **1980**, *72*, 650−654.
(94) Other configurations certainly exist, but due to their weaker or nonexistent H-bond interactions, we anticipate their prevalence in room temperature solution (and in particular their impact for the proton frequency, which is our focus) will be unimportant.
(95) Tomasi, J.; Mennucci, B.; Cammi, R. Quantum Mechanical Continuum Solvation Models. *Chem. Rev.* **2005**, *105*, 2999−3094.
(96) Schmidt, M. W.; Baldridge, K. K.; Boatz, J. A.; Elbert, S. T.; Gordon, M. S.; Jensen, J. H.; Koseki, S.; Matsunaga, N.; Nguyen, K. A.; Su, S. J.; Windus, T. L.; Dupuis, M.; Montgomery, J. A. General Atomic and Molecular Electronic Structure System. *J. Comput. Chem.* **1993**, *14*, 1347−1363.
(97) The dipole moment model in eq 45 is linear in the proton stretch q, a dependence consistent with the observation that the proton charge remains constant as it is moved from proton-donor to proton-acceptor.[77−79]
(98) In principle, both $\mu_{N,o}$ and $\mu_{I,o}$ vary with solvent dielectric constant ε due to the polarization of each VB state's electronic

distribution in the solvent's reaction field. By evaluating $\mu_{N,o}$ and $\mu_{I,o}$ specifically for the $\varepsilon_\infty = 2$ solvent, much of this polarization effect is included, but any further polarization for $\varepsilon > \varepsilon_\infty$ is not. An estimate of this extra polarization using the optimized $\varepsilon_\infty = 2$ solvent equilibrium structures of section 4.1 and calculating μ for different ε values show that this effect changes the dipole moment by only ~5% going from $\varepsilon = \varepsilon_\infty$ to $\varepsilon = 80$. Inclusion of such a solvent polarity ε-dependence makes the dipole moment function $\mu_{N,I}(q,Q)$ ε-dependent, in contrast to an assumption of the derivation of eq 38 of section 3. This extra ε-dependence adds several terms to eq 38 via the derivative of $\mu_{N,I}(q,Q)$ with respect to $1/\varepsilon$. However, because this dependence is minimal, these extra terms are negligible, restoring eq 38.

(99) For the neutral VB potential, $\mu_{N,o}$ of eq 45 is a quantum nuclear-averaged quantity, as defined from eqs 12 and 15. The influence of this averaging on the $\mu_{N,o}$ magnitude (<0.1 D) is, however, negligible compared to that (~0.25−0.5 D) of averaging over different complex configurations (and that due to the removal of charge transfer). We set $\mu_{N,o}$ to a value that ensures that $\mu(q)$ overlaps the PCM dipole calculations of Figure 7 for q~1 Å as a reasonable estimate.

(100) While the dipole moment prescription in section 4.2 is approximate, we view it as a reasonable estimate for $\mu_{N,o}$, $\mu_{I,o}$, and μ because it includes the polarization of both the proton-donor and -acceptor moieties, as well as any polarization induced between them. The key difference between the charge characters of the two VB states is thus the charge transfer between A and B present in the ionic VB state. This perspective is consistent with the Mulliken picture for PT,[34,38,101−103] in which electronically adiabatic PT in an H-bond is primarily viewed as H atom transfer from A to B, in concert with an adiabatic electron transfer from B to A associated with a very large electronic coupling between the two VB states.

(101) Mulliken, R. S. Molecular Compounds and their Spectra. III. The Interaction of Electron Donors and Acceptors. *J. Phys. Chem.* **1952**, *56*, 801−822.

(102) Mulliken, R. S.; Person, W. B. *Molecular Complexes*; Wiley: New York, 1969.

(103) Ratajczak, H. Charge-Transfer Properties of the Hydrogen Bond. I. Theory of the Enhancement of Dipole Moment of Hydrogen-Bonded Systems. *J. Phys. Chem.* **1972**, *76*, 3000−3004.

(104) Kiefer, P. M.; Leite, V. B. P.; Whitnell, R. M. A Simple Model for Proton Transfer. *Chem. Phys.* **1995**, *94*, 33−44.

(105) In accordance with our use of free energies here, we take the proton affinity (PA) as that obtained from ΔG measurements.[106−109] The individual PAs used are[106−109] 204 kcal/mol for DMSO, 371.3 kcal/mol for ethanolate, 342.3 kcal/mol for phenolate, and 336.5 kcal/mol for 2-naphtholate.

(106) NIST Chemistry WebBook. http://webbook.nist.gov/ See also Taft, R. W.; Topsom, R. D. The Nature and Analysis of Substitutent Electronic Effects. *Prog. Phys. Org. Chem.* **1987**, *16*, 1−83 and refs 65−67.

(107) Hunter, E. P. L.; Lias, S. G. Evaluated Gas Phase Basicities and Proton Affinities of Molecules: An Update. *J. Phys. Chem. Ref. Data* **1998**, *27*, 413−656.

(108) Bartmess, J. E.; Scott, J. A.; McIver, R. T., Jr. Scale of Acidities in the Gas Phase from Methanol to Phenol. *J. Am. Chem. Soc.* **1979**, *101*, 6046−6056.

(109) Fujio, M.; McIver, R. T., Jr.; Taft, R. W. Effects on the Acidities of Phenols from Specific Substituent-Solvent Interactions. Inherent Substituent Parameters from Gas-Phase Acidities. *J. Am. Chem. Soc.* **1981**, *103*, 4017−4029.

(110) Luo, Y.-R. *Handbook of Bond Dissociation Energies in Organic Compounds*; CRC Press: Boca Raton, FL, 2003.

(111) The free OH frequency for 2-naphthol (ν_{OH} ~ 3657 cm^{-1}) is an average of the *cis* and *trans* conformers,[112−115] while the free OH frequency for ethanol (ν_{OH} ~ 3676 cm^{-1}) is an average of *anti* and *gauche* conformers.[116,117]

(112) Matsumoto, Y.; Ebata, T.; Mikami, N. Characterizations of the hydrogen-bond structures of 2-naphthol−(H_2O)(n), (n = 0−3 and 5) clusters by infrared-ultraviolet double-resonance spectroscopy. *J. Chem. Phys.* **1998**, *109*, 6303−63011.

(113) Matsumoto, Y.; Ebata, T.; Mikami, N. Structures and Vibrations of 2-naphthol−(NH_3) Hydrogen-Bonded Clusters Investigated by IR-UV Double-Resonance Spectroscopy. *J. Mol. Struct.* **2000**, *552*, 257−271.

(114) Matsumoto, Y.; Ebata, T.; Mikami, N. Photofragment-detected IR spectroscopy (PFDIRS) for the OH stretching vibration of the hydrogen-bonded clusters in the S-1 state—Application to 2-naphthol−B (B = H_2O and CH_3OH) clusters. *J. Phys. Chem. A* **2001**, *105*, 5727−5730.

(115) Kouyama, K.; Miyazaki, M.; Mikami, N.; Ebata, T. IR laser Manipulation of cis↔trans Isomerization of 2-naphthol and its Hydrogen-Bonded Clusters. *J. Chem. Phys.* **2006**, *124*, 054315.

(116) Schrems, O.; Oberhoffer, H. M.; Luck, W. A. P. Infrared Studies of Fluoroalcohol-Base Complexes in the Gas Phase, Carbon Tetrachloride Solutions, and Argon Matrices. *J. Mol. Struct.* **1982**, *80*, 129−134.

(117) Hu, Y. J.; Fu, H. B.; Bernstein, E. R. Infrared Plus Vacuum Ultraviolet Spectroscopy of Neutral and Ionic Ethanol Monomers and Clusters. *J. Chem. Phys.* **2006**, *125*, 154305.

(118) Ebata, T.; Mizuochi, N.; Watanabe, T.; Mikami, N. OH Stretching Vibrations of Phenol-$(H_2O)_1$ and Phenol-$(H_2O)_3$ in the S1 State. *J. Phys. Chem. A* **1996**, *100*, 546−550.

(119) Iwasaki, A.; Fujii, A.; Watanabe, T.; Ebata, T.; Mikami, N. Infrared Spectroscopy of Hydrogen-Bonded Phenol-Amine Clusters in Supersonic Jets. *J. Phys. Chem. A* **1996**, *100*, 16053−16057.

(120) Yamada, Y.; Ebata, T.; Kayano, M.; Mikami, N. Picosecond IR-UV pump-probe spectroscopic study of the dynamics of the vibrational relaxation of jet-cooled phenol. I. Intramolecular vibrational energy redistribution of the OH and CH stretching vibrations of bare phenol. *J. Chem. Phys.* **2004**, *120*, 7400−7410.

(121) Kayano, M.; Ebata, T.; Yamada, Y.; Mikami, N. Picosecond IR-UV pump-probe spectroscopic study of the dynamics of the vibrational relaxation of jet-cooled phenol. II. Intracluster vibrational energy redistribution of the OH stretching vibration of hydrogen-bonded clusters. *J. Chem. Phys.* **2004**, *120*, 7410−7418.

(122) Doi, A.; Mikami, N. Dynamics of hydrogen-bonded OH stretches as revealed by single-mode infrared-ultraviolet laser double resonance spectroscopy on supersonically cooled clusters of phenol. *J. Chem. Phys.* **2008**, *129*, 154308.

(123) The bond dissociation energy for the OH stretch in protonated DMSO was taken from that for H_3O^+. Ab initio calculations (B3LYP/6-311+G**) were performed for protonated DMSO and confirm that the OH stretch frequency for protonated DMSO is similar to that for H_3O^+. For gas phase H_3O^+ properties, see Pople, J. A.; Curtiss, L. A. Theoretical Thermochemistry. 2. Ionization Energies and Proton Affinities of AHn Species (A = C to F and Si to Cl); Heats of Formation of their Cations. *J. Phys. Chem.* **1987**, *91*, 155−162 and ref 124.

(124) Roszak, S. An Ab Initio Configuration Interaction Study of Deprotonation and Dehydrogenation Pathways of the Hydronium Cation. *Chem. Phys. Lett.* **1996**, *250*, 187−191.

(125) Cornell, W. D.; Cieplak, P.; Bayly, C. I.; Gould, I. R.; Merz, K. M.; Ferguson, D. M.; Spellmeyer, D. C.; Fox, T.; Caldwell, J. W.; Kollman, P. A. A Second Generation Force Field for the Simulation of Proteins, Nucleic Acids, and Organic Molecules. *J. Am. Chem. Soc.* **1995**, *117*, 5179−5197.

(126) This artificial maneuver distorts highly excited Q vibrational level patterns, but this is not a problem for the proton frequency ν_{AH}, which is calculated with the ground H-bond vibrational mode in the ground and excited states of the proton. Further, the parametrization of the equilibrium (averaged) H-bond characteristics including the H-bond length and dipole moment, which are key for the proton frequency evaluation, as well as the H-bond frequency, results in reasonable values for the H-bonded complexes (cf. Tables 2 and 7).

(127) The $Q_{eq\infty}$ values in Table 2 are smaller than vacuum Q_{eq0} values due to an increased ionic contribution to the H-bond mode that accompanies solvation. The r_{OO} values in Table 7 are smaller than the vacuum Q_{eq0} values due to the attractive H-bond vibrational

component of the nonbonding Morse eqs B.2 and B.3 noted in Appendix B.
(128) Light, J. C.; Hamilton, I. P.; Lill, J. V. Generalized Discrete Variable Approximation in Quantum Mechanics. *J. Chem. Phys.* **1985**, *82*, 1400−1409.
(129) Choi, S. E.; Light, J. C. Determination of the Bound and Quasibound States of Ar−HCl van der Waals Complex: Discrete Variable Representation Method. *J. Chem. Phys.* **1990**, *92*, 2129−2143.
(130) Because the excited proton stretch level is at an energy comparable to a highly excited ground proton state, H-bond mode state (∼15th excited state), more grid points (75) are used in the H-bond Q direction than in the proton stretch q direction (25).
(131) The step-size is typically <0.01, yielding a ν_{AH} uncertainty of <1 cm^{-1}.
(132) The $\varepsilon = \varepsilon_\infty$=1.5 to 3 range clearly encompasses that ($\varepsilon = \varepsilon_\infty \sim$ 1.7 to 2.6) of the nonpolar solvents used in the experiments[18] (see Table 1). The extra extent of curve displayed in Figure 1 is intended to visually indicate the linearity and the slope magnitude.
(133) The theory's $\varepsilon = \varepsilon_\infty = 1$ proton frequency values have no electronic and orientational polarization contributions, as appropriate for the vacuum H-bonded complex. This provides only an approximate value of that complex's frequency (and thus, also for the shift from the vacuum) because the H-bond structures and potentials used are reasonable estimates *in solution* rather than in vacuum; see discussion in section 4.
(134) A related situation is that the solvent electronic and orientational polarization contributions to the well-known Born solvation free energy[20,21,135] for an ion (which can be obtained by expressing $\{1 - 1/\varepsilon\}$ as $\{(1 - 1/\varepsilon_\infty) + (1/\varepsilon_\infty - 1/\varepsilon)\}$) become nearly identical in the same circumstances.
(135) Bashford, D.; Case, D. A. Generalized Born Models of Macromolecular Solvation Effects. *Annu. Rev. Phys. Chem.* **2000**, *51*, 129−152.
(136) This excellent agreement stems from the minimal (<1%) dipole moment $\langle\mu\rangle_{eq0}$ variation over the ε range (represented in eq 53 by the factor in curly brackets); cf. Table 4.
(137) The shift eqs 55 and 59 are defined relative to the $\varepsilon_\infty = 2$ solvent, while the (different theory-based) shift expressions of Buckingham[22] and Pullin[23−25] are defined relative to the free AH vibration in vacuum.
(138) The average $\langle c_1^2 Q\rangle_{eqn}$ is within 1% of the split average $\langle c_1^2\rangle_{eqn}$ $\langle Q\rangle_{eqn}$ because the H-bond extension is fairly localized. This approximation is used in eq 56 and thus eq 57 to clearly expose the impact of charge transfer.
(139) Pines, E.; Pines, D. Proton Dissociation and Solute-Solvent Interactions Following Electronic Excitation and Photoacids. In *Ultrafast Hydrogen Bonding Dynamics and Proton Transfer Processes in the Condensed Phase*; Bakker, H., Elsaesser, T., Eds.; Kluwer Academic Publishers: Boston, 2003; pp 155−184.
(140) Nibbering, E. T. J.; Fidder, H.; Pines, E. Ultrafast Chemistry: Using Time-Resolved Vibrational Spectroscopy for Interrogation of Structural Dynamics. *Annu. Rev. Phys. Chem.* **2005**, *56*, 337−367.
(141) Tolbert, L. M.; Solntsev, K. M. Excited-State Proton Transfer: From Constrained Systems to "Super" Photoacids to Superfast Proton Transfer. *Acc. Chem. Res.* **2002**, *35*, 19−27.
(142) Pines, E.; Huppert, D. pH Jump: a Relaxational Approach. *J. Phys. Chem.* **1983**, *87*, 4471−4478.
(143) Viappiani, C.; Bonetti, G.; Carcelli, M.; Ferrari, F.; Sternieri, A. Study of Proton Transfer Processes in Solution Using the Laser Induced *pH*-Jump: A New Experimental Setup and an Improved Data Analysis Based on Genetic Algorithms. *Rev. Sci. Instrum.* **1998**, *69*, 270−276.
(144) Zelent, B.; Vanderkooi, J. M.; Coleman, R. G.; Gryczynski, I.; Gryczynski, Z. Protonation of Excited State Pyrene-1-Carboxylate by Phosphate and Organic Acids in Aqueous Solution Studied by Fluorescence Spectroscopy. *Biophys. J.* **2006**, *91*, 3864−3871.
(145) Pines, E.; Huppert, D.; Gutman, M.; Nachliel, E.; Fishman, M. The *p*OH Jump: Determination of Deprotonation Rates of Water by 6-Methoxyquinoline and Acridine. *J. Phys. Chem.* **1986**, *90*, 6366−6370.
(146) Hynes, J. T.; Tran-Thi, T.-H.; Granucci, G. Intermolecular Photochemical Proton Transfer in Solution: New Insights and Perspectives. *J. Photochem. Photobiol., A* **2002**, *154*, 3−11.
(147) Granucci, G.; Hynes, J. T.; Millíe, P.; Tran-Thi, T.-H. A Theoretical Investigation of Excited State Acidity of Phenol and Cyanophenols. *J. Am. Chem. Soc.* **2000**, *122*, 12235−12245.